

ANALYZING TRANSIENT-EVOKED OTOACOUSTIC EMISSIONS BY CONCENTRATION OF FREQUENCY AND TIME

HAU-TIENG WU AND YI-WEN LIU

ABSTRACT. The linear part of transient evoked (TE) otoacoustic emission (OAE) is thought to be generated via coherent reflection near the characteristic place of constituent wave components. Because of the tonotopic organization of the cochlea, high frequency emissions return earlier than low frequencies; however, due to the random nature of coherent reflection, the instantaneous frequency (IF) and amplitude envelope of TEOAEs both fluctuate. Multiple reflection components and synchronized spontaneous emissions can further make it difficult to extract the IF by linear transforms. In this paper, we propose to model TEOAEs as a sum of *intrinsic mode-type functions* and analyze it by a nonlinear-type time-frequency analysis technique called concentration of frequency and time (ConceFT). When tested with synthetic OAE signals with possibly multiple oscillatory components, the present method is able to produce clearly visualized traces of individual components on the time-frequency plane. Further, when the signal is noisy, the proposed method is compared with existing linear and bilinear methods in its accuracy for estimating the fluctuating IF. Results suggest that ConceFT outperforms the best of these methods in terms of optimal transport distance, reducing the error by 10 to 21% when the signal to noise ratio is 10 dB or below.

1. INTRODUCTION

Transient evoked (TE) otoacoustic emissions (TEOAEs) were discovered 40 years ago Kemp (1978). By inspecting the waveforms, TEOAEs generally exhibit a *chirp-like* feature in that the high frequency components seem to occur earlier than low frequency parts. The latency of TEOAE as a function of frequency (hereafter referred to as the *latency function*) could potentially provide valuable information for hearing diagnostic purposes because it is, if not directly proportional to, at least highly correlated with the sharpness of cochlear and psychoacoustic tuning (Neely *et al.*, 1988; Shera *et al.*, 2002, 2010). However, the notion of latency function itself might be an over-simplification of the signal of interest for a few reasons. First, the coherent reflection theory predicts that the phase in TEOAE spectra would fluctuate Zweig and Shera (1995); Talmadge *et al.* (2000) because of the random nature in how the traveling waves are scattered in the cochlea near the characteristic places. The spectrum varies across different ears, and the latency function unavoidably has large deviations if directly derived from the phase gradient (Shera and Bergevin, 2012). Secondly, the reverse traveling waves in the cochlea also get reflected at the stapes, so the OAE waveform measured in the ear canal is a superposition of multiple reflections (e.g., see Fig. 8 of Talmadge *et al.*, 1998). To capture the reflections, we propose that TEOAE signals would be represented better by a sum of *intrinsic mode type (IMT) functions* that each has time-varying amplitudes

TABLE 1. List of abbreviations

AM	Amplitude modulation
BM	Basilar membrane
ConceFT	Concentration of frequency and time
CWD	Choi-Williams distribution
CWT	Continuous wavelet transform
IF	Instantaneous frequency
EMD	empirical mode decomposition
IMT	Intrinsic mode type
iTFR	Ideal time-frequency representation
MT	Multi-taper
RM	Reassignment method
OAE	Otoacoustic emission
OTD	Optimal transport distance
SNR	Signal-to-noise ratio
SFOAE	Stimulus frequency OAE
SOAE	Spontaneous OAE
SPWV	Smoothed pseudo Wigner-Ville distribution
SSOAE	Synchronized spontaneous OAE
SST	Synchrosqueezing transform
STFT	Short-time Fourier transform
TB	Tone burst
TEOAE	Transient evoked OAE
T-F	Time-frequency

modulation and instantaneous frequency. Based on this model, we suggest to analyze TEOAE waveforms by a modern time-frequency (T-F) analysis tool called *concentration of frequency and time* (ConceFT) Daubechies *et al.* (2016).

Modern T-F analysis tools could be roughly classified into three categories, the linear-type, the bilinear-type and the nonlinear-type. The basic ideas behind the linear-type T-F analysis include (i) dividing the signal into segments and evaluating the spectrum for each segment (e.g., the Gabor transform or short-time Fourier transform (STFT)) Flandrin (1999), (ii) measuring the similarity between the signal and a series of dilations of a given mother wavelet, which leads to the continuous wavelet transform (CWT) Tognola *et al.* (1997); Notaro *et al.* (2007), or (iii) the S-transform (ST) Mishra and Biswal (2016) that combines features from STFT and CWT such as frequency modulation and dilation. The bilinear-type T-F analysis catches signal properties from the energy or cross correlation viewpoint, which includes a wide range of methods from the traditional Wigner-Ville distribution to the Cohen class Flandrin (1999). The nonlinear-type T-F analysis aims to depict the signal in a more data-driven way, by either taking more signal information to modify the linear-type or bilinear-type T-F analyses, or extracting the information directly from the signal. This category includes the reassignment method (RM) Auger and Flandrin (1995), the synchrosqueezing transform (SST) Daubechies *et al.* (2011); Wu (2011); Oberlin *et al.* (2015), the empirical

mode decomposition (EMD) Huang *et al.* (1998); Kopsinis and McLaughlin (2009), and several others. We refer the readers to Flandrin (1999) for a general discussion of available methods and Daubechies *et al.* (2016) for a recent review of the field.

Specifically for analyzing TEOAE, Jedrzejczak *et al.* (2009) built a dictionary of asymmetric Gabor functions to span a linear space and applied matching pursuit algorithms to identify the best fit to TEOAEs. The latency function could be inferred and empirical fits were reported. The CWT has been utilized to see the composition or frequency variation of the TEOAE Tognola *et al.* (1997); Notaro *et al.* (2007), to filter the OAE signals Janusauskas *et al.* (2001); Moleti *et al.* (2012), to investigate the relationship of TEOAE latency and stimulus level Sisto and Moleti (2007), and to infer the hearing functionality of neonates (Moleti *et al.*, 2005; Tognola *et al.*, 2001). Because of the multi-resolution property, CWT provides flexibility to analyze the frequency latency structure of the OAEs. By filtering on the T-F plane and then applying the inverse transform, it became also possible to separate the first-reflection component from its mixture with later reflections Shera and Bergevin (2012). Recently, the robustness against noise for various time-frequency techniques was compared using simulated TEOAE data (Biswal and Mishra, 2017), the techniques being compared included STFT, CWT, SST, the S-transform, and EMD; the result suggested that CWT was the most accurate way for estimating the latency function at a signal-to-noise ratio (SNR) of 15 dB.

As elegant as the existing T-F analysis techniques are, however, there are intrinsic difficulties toward a deeper insight into the TEOAE. For the widely applied linear-type T-F analysis, like STFT, CWT and S-transform, the uncertainty principle Flandrin (1999); Ricaud and Torresani (2014) is inevitable. A direct consequence of the uncertainty principle is a blurring of the spectrum, depending on the chosen window and its length. Another limitation is its dependence on the chosen window or mother wavelet and lack of the adaptivity to the signal. For example, while we can take the frequency latency property of TEOAE signal into account and design a mother wavelet to well track that part Tognola *et al.* (1997); Sisto *et al.* (2015), when there are other components in the recording, such as the synchronized spontaneous OAE (SSOAE) (e.g., discussed by Keefe, 2012), we might need another mother wavelet to catch them. In short, how to choose a universal mother wavelet to accomodate signals of different features is in general challenging for the linear method, and this could also challenge the interpretation of the outcomes.

While the bilinear-type T-F analysis has a potential to alleviate these limitations, it suffers from different limitations. For example, while the adaptivity issue is resolved by taking the signal itself as the window in the traditional Wigner-Ville distribution, it is limited by the interference terms when the signal is composed of multiple oscillatory components or time-varying frequency. For other commonly applied Cohen class algorithms, like Choi-Williams distribution (CWD) or Smoothed pseudo Wigner-Ville distribution (SPWV), the same interference issue persists. When choosing windows for smoothing is needed, the same interpretation issue for the linear method still stands. Furthermore, when time information is touched during smoothing, it is difficult to preserve causality.

Among different nonlinear-type T-F analyses, the widely applied EMD lacks of theoretical foundation and might lead to erroneous interpretation and conclusion for real data. RM and SST, on the other hand, have been developed rigorously with theoretical support to handle the traditional T-F analysis limitations. In particular, by taking the phase information of the signal into account, the spectrum is sharpened beyond the blurriness limit caused by the uncertain principle, and the resulting T-F representation is less dependent on the chosen windows Daubechies *et al.* (2011); Wu (2011); Oberlin *et al.* (2015). Depending on how the phase information is used, SST can be classified into first Wu (2011) or second Oberlin *et al.* (2015) order. The first order SST is limited to signals with slowly varying frequency and the second order SST is designed to handle fast varying frequency situation. While it is a nonlinear method, it is shown in Chen *et al.* (2014) that the first order SST is robust to reasonable amount of different types of noise, including the non-stationary and heteroscedastic kinds. However, when the signal to noise ratio (SNR) is low (e.g., below 2 dB), the nonlinear-type T-F analyses in general does not perform well. To sum up, while there have been several T-F analysis techniques, it is still a long lasting challenge to study the TEOAE signal, due to (i) its intrinsic oscillatory structure predicted by theory, (ii) the existence of multiple reflection components or even synchronized spontaneous emissions Keefe (2012), and (iii) the low SNR encountered in practice.

To handle these challenges, in this paper, we explore the possibility of analyzing TEOAEs by ConceFT Daubechies *et al.* (2016), which is a nonlinear-type T-F technique that extends the RM and SST by combining the *multi-tapering (MT)* technique. It has been established that, if the signal of interest can be modeled as a sum of IMT functions satisfying a *well-separated* condition and certain *slow-varying* assumptions, then ConceFT helps produce sharpened traces on the T-F plane that represent the signal and are robust to noise Daubechies *et al.* (2016). The basic idea behind ConceFT is twofold. First, a nonlinear-type T-F analysis is chosen, like SST or RM, and the sharpened time-frequency representation provides higher fidelity to the spectral content of the signal. Second, the effects of noise in OAE measurement are reduced by generalizing the traditional MT technique Percival and Walden (1993); Daubechies *et al.* (2016), which benefits directly from the nonlinearity of the sharpening procedure.

To understand which kind of information ConceFT could accurately extract, we adopt two different models to simulate TEOAE in a controlled manner, so that we can evaluate the performance of ConceFT analysis thoroughly and understand what are the conditions for it to work well on TEOAEs. In one model, the TEOAE spectrum is expressed in terms of a direct integral that takes the presence of irregularity into account Shera and Bergevin (2012); Zweig and Shera (1995). In the other model Liu and Neely (2010), irregularities are present in physical variables such as the basilar-membrane mass, damping coefficients, and stiffness, and TEOAEs are “measured” by time-domain simulation. Lastly, we quantify the performance and compare ConceFT with other T-F analysis tools on a fully simulated signal that we know the ground truth.

The organization of the rest of this paper is as follows. Sec. 2 introduces SST and ConceFT in details. Sec. 3 shows the results of applying SST and ConceFT to analyze

synthetic TEOAE data. Based on the results of simulation, Sec. 4 discusses the effectiveness and limitation of the proposed signal analysis approach. Conclusions are given in Sec. 5.

2. CONCENTRATION OF FREQUENCY AND TIME

Based on the literature review, we understand that a TEOAE signal may contain multiple reflection components or even SSOAEs. We suggest that it would be appropriate to model each component with time-varying amplitude and frequency. To capture these, we resort to the intrinsic mode type (IMT) function Daubechies *et al.* (2011) defined as follows,

$$f(t) = A(t)e^{i\phi(t)},$$

where $A(t)$ and $\phi(t)$ satisfy the following three conditions. The first condition is the *regularity* condition; that is, A and ϕ are smooth enough. The second one is the *boundedness* condition; that is, both $A(t)$ and $\phi'(t)$ are strictly positive and bounded from above. The third one is the *slowly varying* condition; that is, we could find constants $\varepsilon_1, \varepsilon_2 > 0$ so that $|A'(t)| \leq \varepsilon_1|\phi'(t)|$ and $|\phi''(t)| \leq \varepsilon_2|\phi'(t)|$ for all t .¹ We refer to $A(t)$ as the *amplitude modulation* (AM) or amplitude envelope of $f(t)$, $\phi(t)$ the phase function of $f(t)$, and $\phi'(t)$ the (*angular*) *instantaneous frequency* (IF) of $f(t)$. The regularity, boundedness and slowly-varying conditions say that locally an IMT function behaves like a sinusoidal function. The slowly varying IF condition can be slightly relaxed Oberlin *et al.* (2015); Kowalski *et al.* (2018) to accommodate fast varying IF like chirps, but to simplify the discussion, we focus on the slowly varying conditions. Note that this model satisfies the identifiability condition Chen *et al.* (2014); that is, if we could find $a(t)$ and $\psi(t)$ that satisfy $f(t) = A(t)e^{i\phi(t)} = a(t)e^{i\psi(t)}$, then $a(t) = A(t)$, and $\psi(t) = \phi(t)$ up to a global difference of an integer multiple of 2π for all time t . This can be easily seen by taking the absolute value and hence unwrapping the phase. Note that although the IMT function is written in the complex form, it is in general not analytic, since the Fourier transform of an IMT function might not be supported on the positive axis due to the time-varying amplitude and frequency.

We thus model the TEOAE signal as a sum of several IMF functions, with different AM and IF functions. For instance, when only two components are considered, the adaptive harmonic model has the following expression,

$$(1) \quad f(t) = A_1(t)e^{i\phi_1(t)} + A_2(t)e^{i\phi_2(t)},$$

where $A_1(t)e^{i\phi_1(t)}$ may model the dominant first-reflection component of TEOAE and $A_2(t)e^{i\phi_2(t)}$ models the second reflection. In this setup, we need the *frequency separation* condition; that is, $\phi'_1(t) - \phi'_2(t) \geq d > 0$ Wu (2011), or $\phi'_1(t) - \phi'_2(t) \geq d(\phi'_1(t) + \phi'_2(t))$ Daubechies *et al.* (2011). Different linear T-F analysis tool needs different frequency separation properties, depending on the frequency modulation or dilation nature of the T-F analysis; $\phi'_1(t) - \phi'_2(t) \geq d > 0$ is needed if STFT is considered, and $\phi'_1(t) - \phi'_2(t) \geq d(\phi'_1(t) + \phi'_2(t))$ is needed if CWT is considered. The frequency separation condition is

¹ Note that this definition is slightly different from that given in Daubechies *et al.* (2011), where $\varepsilon_1 = \varepsilon_2$, since for a practical signal, like TEOAE, the physical units of $A(t)$ and $\phi'(t)$ might be different. This unit issue could be taken care by ε_1 and ε_2 .

needed for the identifiability condition to be satisfied Chen *et al.* (2014); Oberlin *et al.* (2015); Kowalski *et al.* (2018).

If a TEOAE signal can be modeled as a sum of IMT functions, several modern nonlinear-type T-F analysis tools can be applied with theoretical guarantees. Particularly, we can apply the RM or SST to analyze the TEOAE signal and expect to get the IF and AM information back Daubechies *et al.* (2011).² Further, when the SNR is low, we could consider the MT technique Percival and Walden (1993); Xiao and Flandrin (2007) to stabilize the noise impact. A combination of nonlinear-type T-F analysis tools, like SST, and MT techniques is called *concentration of frequency and time* (ConceFT). The SST and the MT techniques are described next, respectively.

2.1. Synchrosqueezing transform. The basic idea behind SST is taking the phase information hidden inside the chosen T-F representation, like STFT Wu (2011), CWT Daubechies *et al.* (2011) or S-transform Huang *et al.* (2016), and shuffling the T-F representation coefficients to alleviate the blurring effect caused by the uncertainty principle. Specifically, SST is composed of three steps. Below, we discuss SST based on STFT, and the discussion for CWT or S-transform can be found in Daubechies *et al.* (2011); Huang *et al.* (2016). First, for a given properly defined function f , the STFT associated with a window function $h(t)$ is defined by

$$(2) \quad V_f^{(h)}(t, \nu) := \int f(\tau) h(\tau - t) e^{-i2\pi\nu(\tau - t)} d\tau,$$

where $t \in \mathbb{R}$ is the time, $\nu = \omega/2\pi \in \mathbb{R}^+$ is the frequency, h is the window function chosen by the user — a common choice is the Gaussian function, i.e. $h(t) = (2\pi\sigma)^{-1/2} e^{-t^2/2\sigma^2}$, where $\sigma > 0$. To sharpen the spectrogram $|V_f^{(h)}(t, \nu)|^2$, note that the phase information of $V_f^{(h)}(t, \nu)$ is not used. A keen observation made in Kodera *et al.* (1978); Auger and Flandrin (1995); Flandrin (1999) is that the geometric and phase information in the T-F representation allows us to sharpen it.

To motivate this keen observation, consider a simple function $f(t) = Ae^{i2\pi f_0 t}$, where $A, f_0 > 0$. By a direct calculation, $V_f^{(h)}(t, \nu) = A\hat{h}(\nu - f_0)e^{i2\pi f_0 t}$, where $\hat{h} := \mathcal{F}[h(t)]$. Note that the frequency f_0 shows up in the phase of $V_f^{(h)}(t, \nu)$. A naïve idea to obtain the frequency information thus consists of two steps: first, the partial derivative of $V_f^{(h)}(t, \nu)$ associated with t is calculated, which gives $\partial_t V_f^{(h)}(t, \nu) = i2\pi f_0 A\hat{h}(\nu - f_0)e^{i2\pi f_0 t}$, and then the frequency f_0 can be retrieved by a direct division; that is,

$$(3) \quad f_0 = \frac{\partial_t V_f^{(h)}(t, \nu)}{i2\pi V_f^{(h)}(t, \nu)}.$$

²In reality, TEOAE signals are real-valued, and Hilbert transform has been applied to construct an IMT from its real part Keefe (2012). In contrast, the RM or SST methods do not require Hilbert transform to take place because they can handle concurrents IMFs, including the special case of $\cos \phi(t) = \frac{1}{2}(e^{i\phi(t)} + e^{-i\phi(t)})$.

To avoid calculating the numerical derivative $\partial_t V_f^{(h)}(t, \nu)$, note that

$$(4) \quad \partial_t V_f^{(h)}(t, \nu) = -V_f^{(\mathcal{D}h)}(t, \nu) + i2\pi\nu V_f^{(h)}(t, \nu),$$

where $\mathcal{D}h$ denotes the derivative of h with respect to time. We thus have $V_f^{(\mathcal{D}h)}(t, \nu) = i2\pi(\nu - f_0)V_f^{(h)}(t, \nu) = i2\pi A(\nu - f_0)\hat{h}(\nu - f_0)e^{i2\pi f_0 t}$. This observation motivates the definition of the following *reassignment rule* (Wu, 2011, Definition 2.3.12),

$$(5) \quad \omega_f^{(h)}(t, \nu) := \nu - \Im \frac{V_f^{(\mathcal{D}h)}(t, \nu)}{2\pi V_f^{(h)}(t, \nu)},$$

where \Im means taking the imaginary part. Equation (5) is well-defined on every points (t, ν) where $V_f^{(h)}(t, \nu) \neq 0$.

To sharpen the T-F representation of $V_f^{(h)}(t, \nu)$, an intuitive approach is, for each time t , moving all coefficients to the entry associated with the frequency we have interest. This intuition is carried out in SST by the following integration formula (Wu, 2011, Definition 2.3.13):

$$(6) \quad s_f^{(h)}(t, \nu) := \int_{\mathfrak{N}_t} V_f^{(h)}(t, \nu') \delta_{|\nu - \omega_f^{(h)}(t, \nu')|} d\nu',$$

where $\mathfrak{N}_t := \{\nu' : |V_f^{(h)}(t, \nu')| > 0\}$. Equation (6) can be understood as a combination of two steps:

- First, find all entries (t, ν') so that the frequency information provided by $\omega_f^{(h)}(t, \nu')$ is ν , which is embodied in $\delta_{|\nu - \omega_f^{(h)}(t, \nu')|}$.³
- Secondly, gather all non-zero STFT coefficients to the entry (t, ν) by the integration.

In the simple example $f(t) = Ae^{i2\pi f_0 t}$, the non-zero STFT coefficients are all moved to f_0 in $s_f^{(h)}(t, \nu)$, resulting a sharp T-F representation.

As is shown in (Wu, 2011, Theorem 2.3.14), SST can be applied to study IMT functions. For $f(t) = A(t)e^{i\phi(t)}$, the sharpened spectrogram by SST (that is, $|s_f^{(h)}(t, \nu)|^2$) is concentrated on $\phi'(t)/2\pi$ with the AM function $A(t)$ encoded inside. As a result, this technique alleviates the blurring effect caused by the uncertainty principle.

However, when the IF of an IMT function changes rapidly, the outcome of the above-mentioned SST becomes less ideal because the reassignment rule is again “blurred”. Certain improvement has been found by Oberlin *et al.* (2015) via further manipulation of the phase function to accommodate the fast-varying IF; the following reassignment rule was introduced,

$$(7) \quad \Omega_f^{(h)}(t, \nu) = \begin{cases} \omega_f^{(h)}(t, \nu) + Q_f^{(h)}(t, \nu)(t - T_f^{(h)}(t, \nu)) & \text{when } \partial_\nu T_f^{(h)}(t, \nu) \neq 0 \\ \omega_f^{(h)}(t, \nu) & \text{otherwise,} \end{cases}$$

³To make it mathematically rigorous, the delta measure should be replaced by a smooth approximation. We skip the technical detail here for the simplicity.

where

$$Q_f^{(h)}(t, \nu) := \frac{V_f^{(\mathcal{D}\mathcal{D}h)(t, \nu)}(t, \nu)V_f^{(h)}(t, \nu) - (V_f^{(\mathcal{D}h)}(t, \nu))^2}{2\pi i[(V_f^{(h)}(t, \nu))^2 + V_f^{(\mathcal{T}h)}(t, \nu)V_f^{(\mathcal{D}h)}(t, \nu) - V_f^{(\mathcal{T}\mathcal{D}h)}(t, \nu)V_f^{(h)}(t, \nu)]}$$

$$(8) \quad T_f^{(h)}(t, \nu) := t + \Re \frac{V_f^{(\mathcal{T}h)}(t, \nu)}{V_f^{(h)}(t, \nu)},$$

Q_f and T_f are defined when their denominators are not zero, \Re means taking the real part, and $(\mathcal{T}h)(t) := th(t)$. $\Omega_f^{(h)}$ is called the *second-order frequency reassignment rule* Oberlin *et al.* (2015). With this terminology, we may call $\omega_f^{(h)}$ the *first-order frequency reassignment rule* Wu (2011).

With the second-order frequency reassignment rule, the second order STFT-based SST is defined as:

$$(9) \quad S_f^{(h)}(t, \nu) := \int_{\mathfrak{N}_t} V_f^{(h)}(t, \nu') \delta_{|\nu - \Omega_f^{(h)}(t, \nu')|} d\nu'.$$

Again, we may call $s_f^{(h)}(t, \nu)$ the first-order STFT-based SST. Note that, for both first and second order STFT-based SST, we nonlinearly reassign the STFT coefficient *only* on the frequency axis, so the causality of the signal is preserved and hence the reconstruction is possible, although we do not pursue these properties in this work. Yet another property of first-order SST is its robustness to noise of different kinds Thakur *et al.* (2013); Chen *et al.* (2014), while it is nonlinear in nature. The above properties enable us to extract dynamical information of a noisy oscillatory signal, particularly the IF and AM.

In this work, due to the chirp-like behavior of the TEOAE signal, we consider the second-order STFT-based SST for the analysis. With no danger of confusion, we call it SST for simplicity below, unless we specify that it is the first order SST. Note that CWT-based SST can also be considered Daubechies *et al.* (2011) for the analysis, but to simplify the discussion, we focus only on the STFT-based SST.

2.2. Generalized multi-taper. While the first order SST is theoretically shown to be robust to a mild level of noise Thakur *et al.* (2013); Chen *et al.* (2014), when the noise is large, its performance might be jeopardized. While theoretical analysis for other nonlinear-type T-F analysis tools are not available, empirically they are robust only when noise level is mild. In practice, the TEOAE obtained within a limited amount of time could be noisy with a rather small SNR. Thus, a technique to reduce the effect of noise would be desired. In this work, we consider the recently proposed generalized MT technique Daubechies *et al.* (2016) to achieve this goal.

The spirit of the traditional MT technique roots in the law of large numbers. Ideally, from a recorded noisy signal, if we can generate several copies of information composed of the clean component and independent noise, by taking average the clean signal will be enhanced. This intuitive idea is carried out in the following way. With the chosen orthonormal windows, the obtained spectral information associated with the clean signal is almost invariant among windows, while that associated with the noise is independent. For example, take a noisy signal given as $Y = f + \xi$, where f is the

signal we have interest and ξ is the added noise, and take J orthonormal windows h_j , $j = 1, \dots, J$. By the linearity of STFT, we have $V_Y^{(h_j)}(t, \eta) = V_f^{(h_j)}(t, \eta) + V_\xi^{(h_j)}(t, \eta)$, for $i = 1, \dots, J$. When ξ is Gaussian and white, we see that $V_\xi^{(h_j)}(t, \eta)$ and $V_\xi^{(h_k)}(t, \eta)$ are independent when $j \neq k$. While the spectral information associated with $V_f^{(h_j)}(t, \eta)$ depends on h_j , by the linearity of STFT again, $\frac{1}{J} \sum_{j=1}^J V_f^{(h_j)}(t, \eta) = V_f^{(\frac{1}{J} \sum_{j=1}^J h_j)}(t, \eta)$. Therefore, by taking an average, only the spectral information associated with the clean signal is reserved. The T-F representation of SST can be improved by the MT technique by considering

$$(10) \quad M_Y := \frac{1}{J} \sum_{j=1}^J S_Y^{(h_j)}.$$

In Lin *et al.* (2014), the MT technique combined with SST is applied to study the anesthesia depth. The combination of the MT technique and RM is considered in Xiao and Flandrin (2007). Ideally, if there are infinitely many orthonormal functions “well supported” in time and frequency domains, the MT technique would lead us to a low bias and low variance estimator of the clean signal information. However, it has been well studied in Daubechies (1988) that the number of orthonormal functions that are well concentrated in the T-F plane is limited. This fact is understood as the “Nyquist rate” for the T-F analysis.⁴

To conquer the limitation of Nyquist rate and further stabilize the algorithm, the nonlinear nature of SST is considered. How ConceFT generalizes the above-mentioned traditional MT technique could be manifested by directly showing the algorithm. Consider a linear combination of given J orthonormal windows h_j , $j = 1, \dots, J$, $h = r^*H$, where $H = [h_1, \dots, h_J]^T$, $r = [r_1, r_2, \dots, r_J] \in \mathbb{C}^J$ and $|r| = 1$, we could obtain a T-F representation, denoted as $S_Y^{(h)}$, by applying the SST. Note that when $r = e_j$ is the unit vector with the j -th entry equal to 1, $r^*H = h_j$. The T-F representation based on ConceFT is defined as

$$(11) \quad C_Y := \frac{1}{N} \sum_{n=1}^N S_Y^{(h_{(n)})}$$

where $r_{(n)}$ is uniformly sampled from the unit sphere in \mathbb{C}^J and $h_{(n)} := r_{(n)}^*H$.

Intuitively, due to the nonlinear nature of SST, the level of dependence is reduced between noise components coming from non-orthogonal windows. Thus, by taking average, the noise could be further canceled. To appreciate the importance of the nonlinearity, take the following examples into account. If we consider the linear-type T-F analysis, like the STFT, and follow the above-mentioned argument regarding

⁴ The “Nyquist rate” here is different from the common Nyquist rate encountered in the sampling theory. Here, it is called the Nyquist rate to describe limited possible windows under the constraints such as orthonormality and well concentration. See Daubechies (1988) for a full development and (Daubechies *et al.*, 2016, ESM-4) for a summary.

generalized MT, we have

(12)

$$\lim_{N \rightarrow \infty} \frac{1}{N} \sum_{n=1}^N V_Y^{(h(n))} = \lim_{N \rightarrow \infty} \frac{1}{N} \sum_{n=1}^N \sum_{j=1}^J e_j^\top r(n) V_Y^{(h_j)} = \sum_{j=1}^J \left[\lim_{N \rightarrow \infty} \frac{1}{N} \sum_{n=1}^N e_j^\top r(n) \right] V_Y^{(h_j)} = 0$$

due to the linearity of STFT. Here we use the fact that

$$\lim_{N \rightarrow \infty} \frac{1}{N} \sum_{n=1}^N e_j^\top r(n) = e_j^\top \int_{x \in \mathbb{C}^J; \|x\|=1} x dx = 0.$$

Further, if we apply the generalized MT to the spectrogram, we have

$$\begin{aligned} \lim_{N \rightarrow \infty} \frac{1}{N} \sum_{n=1}^N |V_Y^{(h(n))}|^2 &= \lim_{N \rightarrow \infty} \frac{1}{N} \sum_{n=1}^N \left| \sum_{j=1}^J e_j^\top r(n) V_Y^{(h_j)} \right|^2 \\ &= \sum_{j=1}^J \left[\lim_{N \rightarrow \infty} \frac{1}{N} \sum_{n=1}^N |e_j^\top r(n)|^2 \right] |V_Y^{(h_j)}|^2 + \sum_{j \neq k}^J \left[\lim_{N \rightarrow \infty} \frac{1}{N} \sum_{n=1}^N (e_j^\top r(n))^* e_k^\top r(n) \right] V_Y^{(h_j)*} V_Y^{(h_k)} \\ &= c \frac{1}{J} \sum_{j=1}^J |V_Y^{(h_j)}|^2, \end{aligned}$$

for some constant $c > 0$, where the last equality comes from the fact that

$$\lim_{N \rightarrow \infty} \frac{1}{N} \sum_{n=1}^N |e_j^\top r(n)|^2 = \int_{x \in \mathbb{C}^J; \|x\|=1} |x_j|^2 dx = c$$

and $\lim_{N \rightarrow \infty} \frac{1}{N} \sum_{n=1}^N (e_j^\top r(n))^* e_k^\top r(n) = \int_{x \in \mathbb{C}^J; \|x\|=1} x_j^* x_k dx = 0$ due to the symmetry since $j \neq k$. Thus, the generalized MT technique leads to the traditional MT on the spectrogram. The same discussion holds for CWT and scalogram.

However, the situation is different when we apply the generalized MT technique to any nonlinear-type T-F analysis. For example, due to the nonlinearity of the SST, $\lim_{N \rightarrow \infty} C_Y$ is not proportional to M_Y , since $S_Y^{(h(n))} \neq \sum_{j=1}^J e_j^\top r(n) S_Y^{(h_j)}$. In brief, due to the Nyquist rate limitation, we choose a reasonably small J , and count on a large N to reject the noise. Although a complete theoretical quantification is still under study, a partial theoretical result and numerical evidence in Daubechies *et al.* (2016) show that the level of dependence between noise components caused by two non-orthonormal windows is reduced after SST. As a result, $\lim_{N \rightarrow \infty} C_Y$ is much closer to S_f than M_Y is, when measured by the optimal transportation distance Daubechies *et al.* (2016). We also mention that the generalized MT technique could be applied to other nonlinear-type T-F analysis, like RM.

In practice, we choose h_1, \dots, h_J to be the first J orthonormalized Hermite functions because they are the most concentrated windows in the T-F domain Daubechies (1988); Daubechies *et al.* (2016). In particular, h_1 is the Gaussian function. In practice, J could be chosen as small as 2, while N could be chosen as large as the user wishes, but a number of $N = 30$ to 100 is in general good enough (e.g. Daubechies *et al.*, 2016).

3. COMPARISON OF VARIOUS WAYS TO ANALYZE TEOAE DATA

In this section, we report results of analyzing simulated TEOAE data by synchrosqueezing and ConceFT. The performance will be compared against what can be achieved by linear analysis methods, including STFT and CWT, and bilinear methods like CWD and SPWV.

3.1. Direct simulation of coherent reflection. This section follows Zweig and Shera's *coherent reflection* approach to simulate a TEOAE signal (1995). Essentially, the TEOAE is regarded as the summation of reflected waves caused by mechanical irregularities throughout the entire length of the cochlea, which is treated as a one-dimensional waveguide. Via Wentzel-Kramers-Brillouin (WKB) approximation Schroeder (1973), Zweig and Shera showed that the amount of reflection can be computed by introducing the irregularities to the wave propagation equation as a perturbation term. This framework successfully explained the periodic fine structure in the spectrum of different types of OAEs and the hearing threshold Talmadge *et al.* (1998). Here, we borrow a phenomenological equation that stems from the 1995 work for *synthesizing* a TEOAE signal without discussing the details of micromechanics of the cochlea. The reflection of traveling waves in the cochlea due to unknown irregularities $\epsilon(x)$ is written as follows (Talmadge *et al.*, 2000; Shera and Bergevin, 2012; Biswal and Mishra, 2017),

$$(13) \quad R(\omega) = \int \epsilon(x') e^{\frac{-(x'-x_p)^2}{2(\Delta x)^2}} e^{-i4\pi \frac{x'-x_p}{\Lambda}} dx',$$

where $\omega > 0$, Δx represents a spatial spread of a traveling wave near its characteristic place, and Λ denotes the local wavelength. Here, $R(\omega)$ represents a reflectance spectrum “seen” from the stapes ($x = 0$) into the cochlea. In the equation, x_p denotes the *characteristic place* of (angular) frequency ω and is assumed to decrease against ω in a log-linear way as follows (Greenwood, 1990),

$$(14) \quad x_p(\omega) = l \log \frac{\omega_0}{\omega},$$

where l is treated as a constant here, and ω_0 is the characteristic frequency at $x = 0$. In Eq. (13), the factor $\exp\left(\frac{-(x'-x_p)^2}{2(\Delta x)^2}\right)$ describes the relative gain a small wave component receives by going from $x = 0$ to $x = x'$ and reflected to travel back to $x = 0$, and the factor $\exp\{-i4\pi(x' - x_p)/\Lambda\}$ corresponds to the phase-shift thereof. In Eq. (13), $R(\omega)$ is zero if $\epsilon(x) = 0$, meaning that TEOAE would not exist if the cochlea were to be perfectly smooth.

By fitting experimental data, it has been found that Δx and Λ should both vary slowly against ω (Shera and Bergevin, 2012). Here, however, we set both of them as constants; in other words, we made a crude simplification of cochlear mechanics so the model has a global scaling symmetry.

Also, we regard the inverse Fourier transform⁵ $r(t) = \mathcal{F}^{-1}[R(\omega)](t)$ as a impulse response, which can be convolved with any transient acoustic stimulus to calculate

⁵ The inverse Fourier transform was calculated via a 4096-point inverse fast Fourier transform with a sampling rate of 32 kHz.

the first-reflection OAE evoked by the stimulus.⁶ Thus, we ignore multiple internal reflection in the cochlea due to impedance mismatch at the stapes. The frequency response of reverse middle-ear transmission, the ear-canal acoustics, and the acoustic properties of the probe termination are also ignored, too.

The model in Sec. 3.2 will consider both the multiple reflections in the cochlea and the middle-ear transmission, and restrict scaling symmetry to be valid only locally. Here in Sec. 3.1, the reason for making these crude simplifications are two-fold. First, we shall see that the first-reflection component already demonstrates fluctuating AM and IF and presents a challenge for data analysis. Therefore, we shall use the synthesized $r(t)$ to help determining ConceFT parameters empirically. Secondly, the global-symmetry assumption happens to allow certain approximations that lead a simpler expression for $r(t)$. It turns out that the level of temporal fluctuation in the AM and IF of $r(t)$ closely depends on the ratio $\Delta x/\Lambda$. Details of mathematical derivation are given in Appendix B, C, and D, and related discussion will be given in Sec. 4.

3.1.1. Choosing the SST and MT parameters. An example of $R(\omega)$ was synthesized via Eq. (13) with the following parameters: $l = 0.72$ cm, $\Lambda = l/5.5$ (Shera and Bergevin, 2012), and $\Delta x = \Lambda/2$. The irregularity function $\epsilon(x)$ was generated by a zero-mean Gaussian random process with a constant variance $E[\epsilon(x)]^2 = \sigma_\epsilon^2$ and no spatial correlation; i.e., $E\{\epsilon(x)\epsilon(x')\} = 0$ if $x \neq x'$. The integral with respect to x' in Eq. (13) was approximated by discretizing along the x' direction from $x' = 0$ to 35 mm with a step size of 5 μ m. The resulting $R(\omega)$ was calculated in the frequency domain from 0.2 to 16 kHz and the inverse fast Fourier transform was applied to obtain the TEOAE signal $r(t)$ sampled at $f_s = 32$ kHz. Then, $\Re\{r(t)\}$ was subject to further analyses. To test the robustness of the signal-processing methods, Gaussian white noise $\xi(t) \sim \mathcal{N}(0, \sigma_\xi^2)$ was added to $\Re\{r(t)\}$. Figure 1 shows $\Re\{r(t)\}$ before and after contaminated by the noise. This signal is further analyzed as below.

An STFT spectrogram $V_f^{(h)}$ of signal $f(t) = \Re\{r(t)\}$ was calculated using the Gaussian window function $h(t)$ with $\sigma = (5\text{ms})/12$. Then, both the 1st-order and the 2nd-order SST were tried for comparison purposes, and the resulting T-F representations $S_f^{(h)}(t, \nu)$ are shown in Fig. 2A and B. The *expected* instantaneous frequency (EIF) function is plotted in Fig. 2C as a reference; The EIF function, denoted as $\bar{\nu}(t)$, is essentially defined as the inverse function of the expected group delay⁷ given by Eq. (23); to be exact, we define that $E\{\tau_g(2\pi\bar{\nu}(t))\} = t$, and therefore,

$$(15) \quad \bar{\nu}(t) = \frac{1}{2\pi} \frac{4\pi}{t} \left(\frac{l}{\Lambda} \right) = \frac{2}{t} \left(\frac{l}{\Lambda} \right) = 11.0/t,$$

where the unit of t is sec and the unit of $\bar{\nu}$ is Hz.

Note that in Fig. 2A and B, both the 1st and the 2nd order SST produce traces that generally follow Eq. (15) but with blurring and deviation. The background is clean in both cases because the noise has not been added yet. Also note that, compared to the 1st-order SST, the trace in the 2nd-order SST appears to be more concentrated when

⁶Of course, this would no longer be valid if nonlinearity in cochlear mechanics is considered.

⁷In human data, the inverse relation was find to hold for a limited period of time, from about $t = 3$ to 8 ms Keefe (2012).

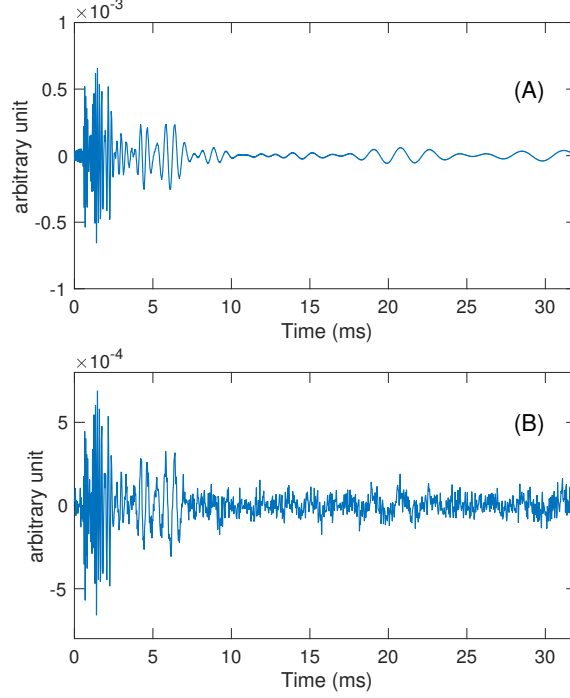


FIGURE 1. Signals generated by Eq. (13) for further analysis. (A) the real part of the clean TEOAE signal $r(t)$. (B) Contaminated by Gaussian noise with $\sigma_\xi = 4.7 \times 10^{-5}$.

the IF changes fast, as was predicted by the established theorem Daubechies *et al.* (2011); Oberlin *et al.* (2015). For this reason, the 2nd-order SST is chosen as the tool for analyzing the signals further.

Fig. 2D shows the 2nd-order SST of the contaminated signal $f(t) = \Re\{r(t)\} + \xi(t)$ (See Fig. 1B). By inspection and comparing with Fig. 2B, we can find several spurious traces in the upper-right hand side of the “main trace” due to the additive noise (the main trace is vaguely defined as the set of all visible traces located close to $\nu = \bar{\nu}(t)$ on the T-F plane). Fig. 2E and F show the result of further processing by ConceFT using the first $J = 2$ and 3 Hermite basis functions, respectively. The number of averages in Eq. (11) is $N = 90$. Note that, before time $t = 10$ ms, the main trace appears to be preserved in both Fig. 2E and F. At time $t > 10$ ms, however, the main trace appears to be harder to identify, especially between $t = 10$ and 13 ms. In fact, the global scaling symmetry assumption in this model predicts that the TEOAE amplitude would decay fast; and we attempt to provide a mathematical explanation for the reasons in Appendix D. Consequently, it becomes harder to see the tracing at later time as the signal level eventually drops beneath the noise floor.

Also note that the spurious traces due to the presence of noise appear to be suppressed better when using $J = 3$ Hermite functions (Fig. 2F) than $J = 2$ (Fig. 2E), and this improved performance possibly comes with the price of lowering the visibility of the main trace when the SNR is below a certain limit, e.g., around $t = 12$ and also $t = 17$ ms, respectively.

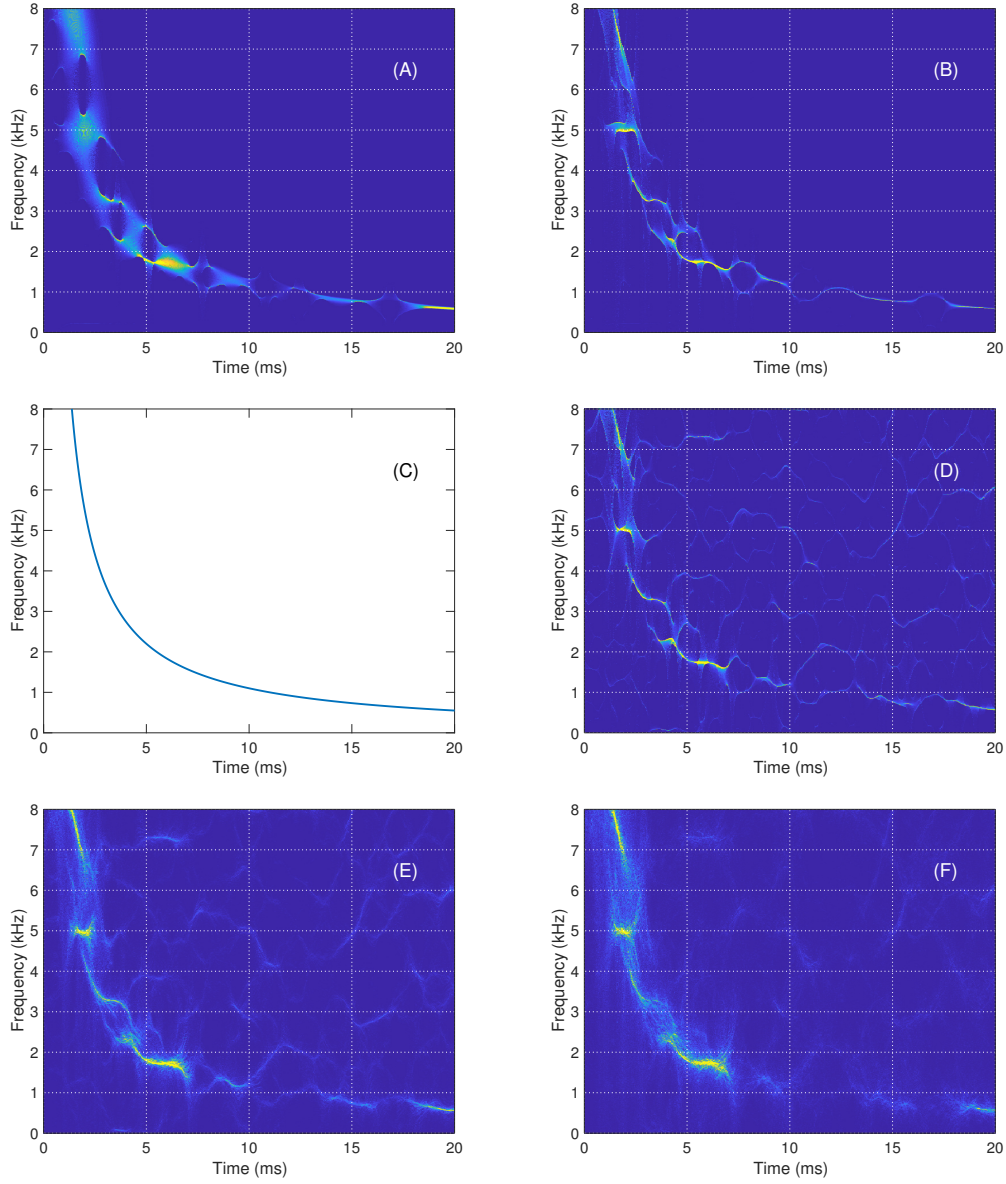


FIGURE 2. (Color online) Results of representing simulated TEOAE signals by SST and ConceFT. **(A)** 1st-order SST, clean signal. **(B)** 2nd-order SST, clean signal. **(C)** The *expected* instantaneous frequency (see Eq. 15 for the definition) as a function of time. **(D)** 2nd-order SST, noise contaminated. **(E)** ConceFT with $J = 2$ and $N = 90$. **(F)** ConceFT with $J = 3$ and $N = 90$.

3.1.2. *Results with a more realistic value of $\Delta x/\Lambda$.* Based on Eq. (13), we will show in Appendix B and C that the OAE signal, $b(t)$, evoked by a narrowband stimulus $g(t)$

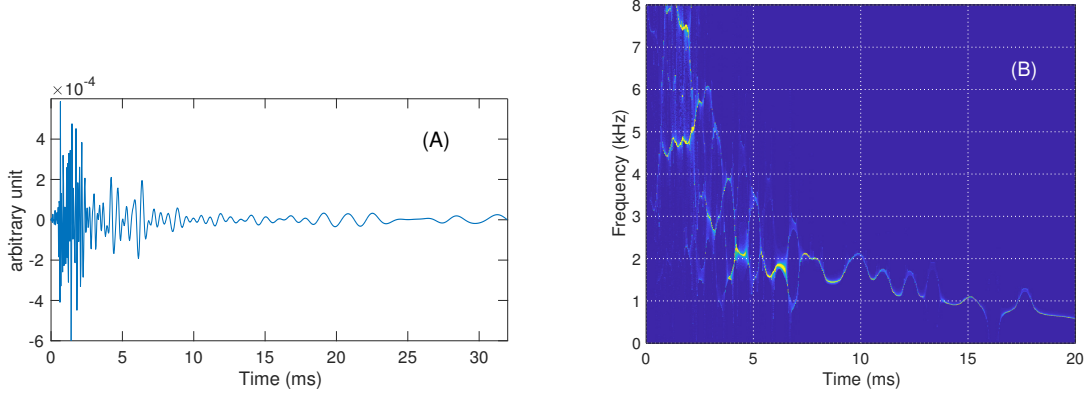


FIGURE 3. (Color online). Results with a more realistic value of Δx . **(A)** $r(t)$ with $\Delta x = l/(\sqrt{2\pi}10) \approx 0.22\Lambda$, as in Shera and Bergevin (2012) and Biswal and Mishra (2017). **(B)** the corresponding 2nd-order SST, obtained with a Gaussian window $\sigma = 0.167$ ms.

that is centered around frequency ω_b could be approximated as follows,

$$(16) \quad b(t) \approx C'' R(\omega_b) \cdot g \left(t - \frac{4\pi}{\Lambda} \frac{l}{\omega_b} \right),$$

where $C'' = e^{i\frac{4\pi}{\Lambda}l}$ represents a constant phase shift that does not depend on ω_b , and $R(\omega_b)$ depends on the irregularity function $\epsilon(x)$ is given by Eq. (13). However, the goodness of approximation of Eq. (16) relies on $\Delta x/\Lambda$ being sufficiently large, and it can be expected that the behaviors of TEOAE become more difficult to capture when $\Delta x/\Lambda$ is low. The goodness of approximation by Eq. (16) and implications will be further discussed in Sec. 4.

Fig. 3 shows the result of simulating $r(t)$ with a more reasonable value of $\Delta x/\Lambda$ (Shera and Bergevin, 2012; Biswal and Mishra, 2017) inferred from experiments (Rhode, 1978). To simplify the discussion, no noise is added in this example. By inspection, the amplitude variation in Fig. 3A looks more irregular than Fig. 1A. Moreover, the result of SST in panel (B) indicates that the IF also changes rapidly; in practice, this turns out to be difficult to capture, and thus a shorter window was selected so as to obtain a clear plot.

3.2. TEOAE from a cochlear model with electromotile outer hair cells. It has been shown in simulations that a computer cochlear model could generate TEOAE or SFOAE if random perturbation is introduced to some physical parameters along x (Choi *et al.*, 2008; Verhulst *et al.*, 2012). In this section, we adopt a model that captures certain bio-mechanical details of cochlear mechanics Liu and Neely (2010) so that irregularities can be placed in physically meaningful parameters. Then, by attaching a middle-ear model to the cochlear model and terminating with an enclosed ear canal Liu and Neely (2010), one can simulate multiple reflections of the traveling waves so that the OAE signal becomes a superposition of multiple components, unlike the single-component formulation described so far. We shall see that the model also

exhibits SSOAEs if the level of roughness is set sufficiently high. The simulated OAE data “measured” in the ear canal are then subject to various ways of linear and nonlinear analysis so performance of different methods can be compared in Sec. 3.3.

The adopted model was based on an earlier transmission-line model of cochlear mechanics Neely (1985, 1993) but the outer hair cell (OHC) “modules” were replaced by a piezoelectrical equivalent circuit Mountain and Hubbard (1994); Liu and Neely (2009) to account for OHC somatic motility. The mechano-electrical transduction current of the OHCs were also made to saturate so the entire system becomes nonlinear Liu and Neely (2010). However, in the past, the model parameters have been intentionally designed to vary smoothly so it did not generate stimulus-frequency OAEs at a significant level Liu and Liu (2016). In the present research, we added roughness to the model by introducing randomness in the following way,

$$(17) \quad m_b(x) = m_b^{(0)}(x)(1 + \epsilon(x)),$$

where m_b denotes the basilar-membrane (BM) mass density, $m_b^{(0)}(x)$ denotes its mean values before introducing roughness, and $\epsilon(x) \sim \mathcal{N}(0, \sigma_\epsilon^2)$ as in Sec. 3.1. Choi *et al.* showed that spectral filtering of $\epsilon(x)$ affects the level and spectral composition of coherent reflection-based OAEs. In the present work, once an instance of completely random $\epsilon(x)$ is generated, it is subject to moving-average smoothing so that the spatial correlation function $\kappa(x, x') = \mathbb{E}\{\epsilon(x)\epsilon(x')\}$ is given as follows,

$$\kappa(x, x') = \sigma_\epsilon^2 \cos^2 \frac{\pi(x - x')}{2D},$$

if $|x - x'| \leq D$, and $\kappa(x, x') = 0$ otherwise. Figure 4 shows an example of TEOAE obtained from this model, measured in the ear canal. The stimulus is a wide-band click with a peak amplitude of 5.8 mPa. The stimulus actually generates ear-canal ringing for the first two milliseconds or so. Therefore, we conveniently calculated the response with and without roughness in the cochlea, so that the ringing effect can be removed by taking the difference because it is mainly due to the linear responses of the ear canal and the middle ear. What is shown in Fig. 4 is the difference signal, which can be regarded as an accurate estimate of the true emissions since the original model is known to generate negligible TEOAEs without roughness Liu and Liu (2016).

The parameters for the roughness function are $\sigma_\epsilon = 0.03$, and $D = 0.3$ mm. Empirically, increasing σ_ϵ and decreasing D tends to increase the level of TEOAEs. In this particular example, apparently, there is a long-lasting high frequency component during $t = 16$ to 32 ms, which can be made to disappear by using a lower value of σ_ϵ in simulation. Empirically, at $\sigma_\epsilon > 0.4$ the model begins to produce self-sustained oscillation inside the cochlea and spontaneous OAE (SOAE) in the ear canal. We have not conducted a thorough search for the criteria for SOAE to happen in the model, as it is outside the scope of this paper. The signal in Fig. 4 is used for comparing different T-F analysis methods, to be described next.

3.3. Comparing different T-F representations. We compare ConceFT with commonly used T-F analyses, including STFT, CWT, CWD, and SPWV. For reproducibility, a publicly available toolbox called Time-Frequency Toolbox (TFTB) (<http://>

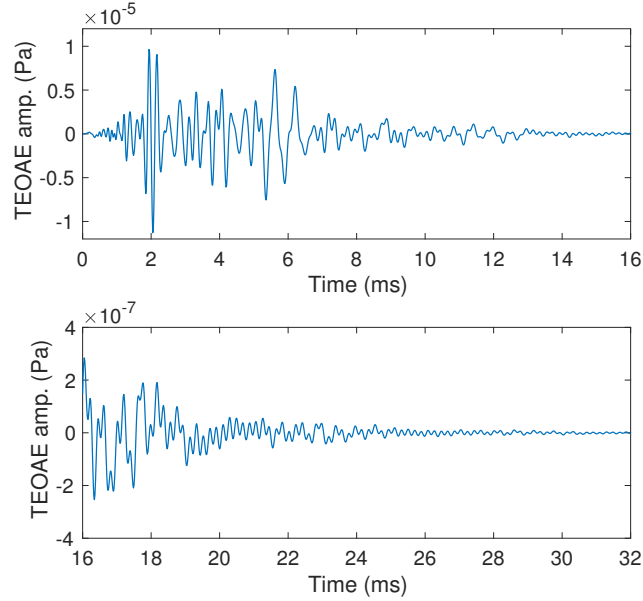


FIGURE 4. An example of TEOAE obtained by introducing roughness to the Liu and Neely (2010) model. The stimulus is a wide-band click with peak amplitude at 5.8 mPa. The parameters for simulation are $\sigma_\epsilon = 0.03$, and $D = 0.3$ mm.

tftb.nongnu.org) is used for the STFT, CWT, CWD, and SPWV. The code of ConceFT is available in the authors' website (<https://hautiengwu.wordpress.com/code/>). For the CWT, we use a suggested mother wavelet in previous papers Tognola *et al.* (1997); Sisto *et al.* (2015). For STFT, SST and ConceFT, we apply the same window length for a fair comparison. For STFT and SST, the Gaussian window is considered, and for ConceFT, the Gaussian window and the first Hermite window is considered. For CWD and SPWV, the length of the time smoothing window is chosen to be the same as the window for STFT, and the length of the frequency smoothing window is chosen to be 2.5 times the length of the time smoothing window, as is suggested in the TFTB code. Since the scalogram (the squared modulation of CWT), CWD and SPWV are bilinear in nature, to have a fair comparison, the squared modulation of SST, $|s_f^{(h)}(t, \nu)|^2$, and the squared modulation of ConceFT, $|C_Y(t, \nu)|^2$ (see Eq. 11 for definition), are displayed.

3.3.1. Results of analyzing TEOAE and SSOAE generated by the Liu and Neely (2010) model: visual comparison. The results of analyzing the signal in Fig. 4 by different methods are shown in Fig. 5 for visual comparison. All the T-F representation are able to capture the main trace dropping from 6 kHz to 2 kHz and below in the first 10 ms. The main trace supposedly represents the first-reflection component of TEOAE. Beside the main trace, a few other traces are noteworthy in SST and ConceFT; first, we see that a trace near 5.0 kHz can be easily captured in SST or ConceFT. The trace extends over 20 ms and is especially visible in ConceFT, and it certainly corresponds

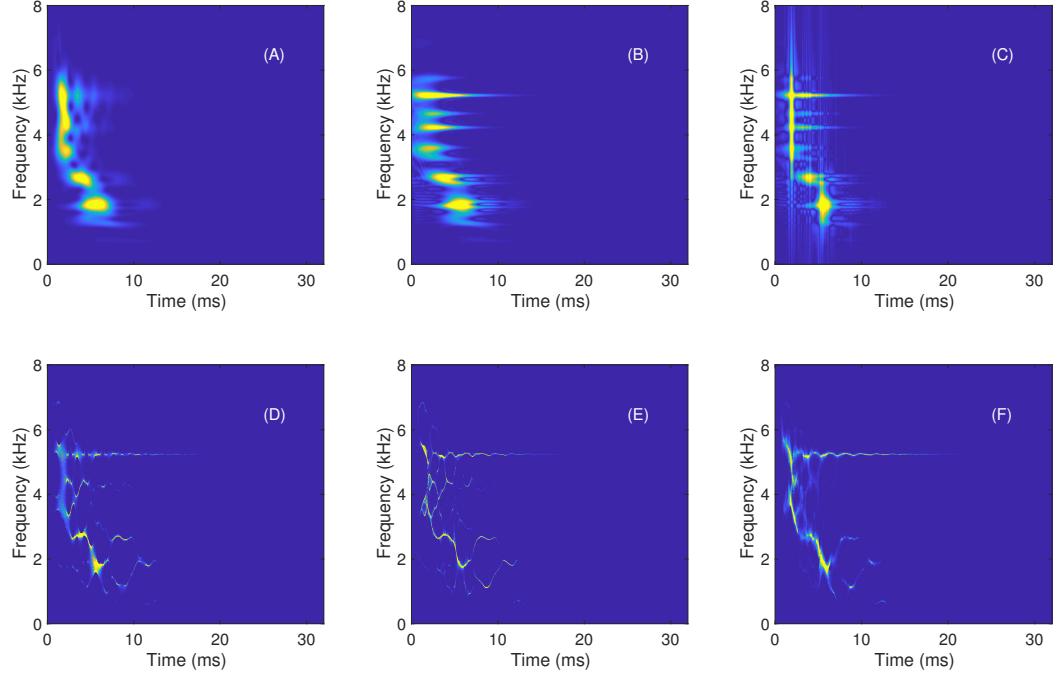


FIGURE 5. (Color online). T-F representations of a clean signal by different algorithms. The signal in Fig. 4 is analyzed by (A) scalogram, (B) SPWV, (C) CWD, (D) squared modulation $|s_f^{(h)}(t, \nu)|^2$ of the 1st-order SST, (E) squared modulation of the 2nd-order SST, and (F) squared modulation of ConceFT, respectively.

to the long tail in Fig. 4 which extends to time > 25 ms. We refer to this long-lasting component as the SSOAE here. In contrast, in the scalogram, SPWV, and CWD, the component is not as easy to identify. Note that the 5-kHz component in the scalogram looks like “wideband”. This is because in the frequency domain the mother wavelet is wide in the high frequency region due to the dilation nature of the CWT.

Secondly, to the right of the main trace in SST and ConceFT, we arguably see a second trace at doubling the time. For instance, near $t = 8.4$ ms a component at 2.7 kHz re-occurs (after its first occurrence near $t = 4.2$ ms), and arguably that component drops to 1.8 – 1.9 kHz at around $t = 11.4$ ms. Based on hindsight, since the Liu and Neely model consists of the middle-ear part and the cochlear part, it should not be surprising to see multiple reflections due to the impedance mismatch at the stapes. Hence, this second trace at doubling the latency likely represents the second-reflection component of TEOAE. Note that the component is also visible in the scalogram, as it has been reported when analyzing synthetic data generated by a model with internal reflection (Shera and Bergevin, 2012, their Fig. 10); previously, the linearity of CWT

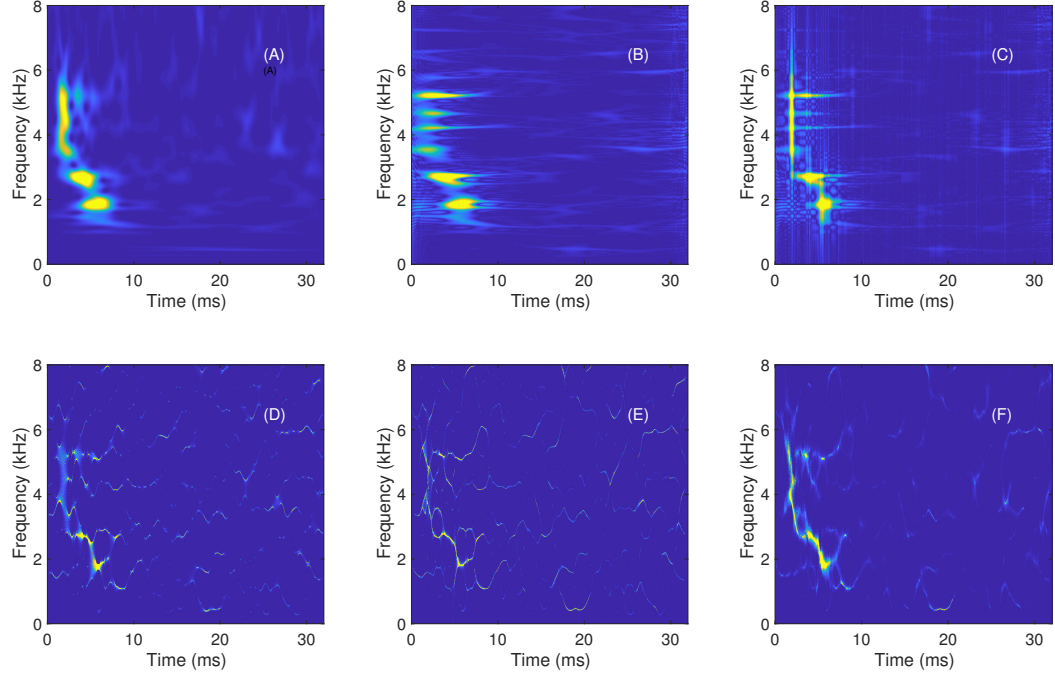


FIGURE 6. (Color online). T-F representations of the same signal as Fig. 5 but at SNR = 0 dB by (A) scalogram, (B) SPWV, (C) CWD, (D) squared modulation $|s_f^{(h)}(t, \nu)|^2$ of the 1st-order SST, (E) squared modulation of the 2nd-order SST, and (F) squared modulation of ConceFT, respectively.

conveniently allowed separation of reflection components by masking out part of the T-F representation and applying the inverse transform. The component, however, seems not so visible in bilinear transforms (SPWV and CWD) for this particular example.

To further examine the performance of ConceFT at low SNR region, we add a Gaussian white noise to the signal, with the SNR = 0 dB calculated over the entire time (32 ms). The result is shown in Fig. 6. As can be visualized, even when the SNR is so low, the SSOAE component can still be identified with ConceFT. Although the SSOAE component now appears to be blurred in ConceFT, it is still more “concentrated” than in the CWT. The main trace remains robust against the noise in all 6 representations, while the trace appears brighter in ConceFT than in SST. Comparing (D) and (E) to (F), we also see that the noise seems to be more successfully ignored by ConceFT than by 1st-order and 2nd-order SST, which demonstrates the effectiveness of multi-tapering in providing robustness against additive noise.

3.3.2. Results of analyzing a three-component, OAE-like synthetic signal: Comparison by optimal transport distance. To facilitate quantitative comparison between the performance of different T-F analysis methods, we synthesized an OAE-like signal with

TABLE 2. Recovery of the iTFR by different T-F analysis methods. Performance is evaluated by the optimal transport distance (a smaller distance means a better recovery). The mean and standard deviation of 30 realizations of noise is reported. SPWV: smooth pseudo Wigner Ville distribution; CWD: Choi-Williams distribution; 1-st SST: the squared modulation of the first order SST; SST: the squared modulation of the second order SST; ConceFT: the squared modulation of concentration of Frequency and Time.

SNR	scalogram	SPWV	CWD	1st-SST	SST	ConceFT
100 dB	2.27 (0.00)	2.03 (0.00)	2.93 (0.00)	0.69 (0.00)	0.83 (0.00)	1.20 (0.07)
10 dB	3.29 (0.11)	3.34 (0.12)	3.55 (0.08)	2.65 (0.13)	2.75 (0.12)	2.61 (0.14)
5 dB	3.53 (0.11)	3.61 (0.14)	3.73 (0.09)	3.02 (0.14)	3.11 (0.13)	3.00 (0.14)
2 dB	3.65 (0.11)	3.73 (0.12)	3.84 (0.08)	3.23 (0.13)	3.30 (0.12)	3.21 (0.14)
0 dB	3.72 (0.11)	3.81 (0.11)	3.90 (0.09)	3.36 (0.13)	3.42 (0.13)	3.35 (0.14)

the following specification. Let $F_{a,b,c}(t) = a + \frac{S_c\{W(s)\}}{b \max_{0 \leq s \leq L}(S_c\{W(s)\})}$ denote a time function with length L , mean $a > 0$ and $b > 0$ and perturbed by the standard Brownian motion $W(s)$ with $W(0) = 0$ Yakov (1992), and S_c is the locally weighted smoothing operator of kernel bandwidth $c > 0$. A signal consisting of three oscillatory components was produced, each with a time-varying amplitude and frequency. The first component is a chirp-like signal with frequency dropping from 8000 to 2000 Hz following the $1/t$ rule, which lasts from 1 ms to 20 ms. This component simulates the TEOAE component. The phase $\phi_1(t)$ is a realization of $1000(2\pi) \times (\frac{120}{19} \log(t/1\text{ms}) + \frac{13}{19}(t-1) + F_{1,6,0.3})$. The second component oscillates around frequency 5000 Hz, which lasts from 2ms to 25 ms. This component may simulate an SSOAE-like component. The phase $\phi_2(t)$ is a realization of $1000(2\pi)(5t + 0.1 \cos(\pi t) + F_{0,5,0.4})$. The third component oscillates around 3141 Hz, which lasts from 3 ms to 10 ms. It may simulate another SSOAE-like component. The phase is $\phi_3(t) = 3141(2\pi)t$. The amplitude of the three components, $A_1(t)$, $A_2(t)$ and $A_3(t)$, are realizations of $F_{1,2,0.2}$, $F_{1/2,4,0.1}$, and $F_{1/3,6,0.1}$ respectively. Note that a realization of $F_{a,b,c}$ is a smooth function and due to its random nature it is not easy to express it by any well known function, which makes this evaluation somewhat realistic.

The signal is sampled at 32000 Hz, and the SNR ranges from 100 to 0 dB. We then apply ConceFT, SST, CWT, CWD, and SPWV to the simulated signal. To evaluate the performance of different T-F analyses on this signal, we define the “ideal T-F representation (iTFR)” in the following way — suppose the signal is $f(t) = \sum_{l=1}^3 A_l(t)e^{i\phi_l(t)}$. The iTFR is defined as follows,

$$(18) \quad R(t, \omega) = \sum_{l=1}^3 A_l(t) \delta(\omega - \phi'_l(t)),$$

where $\delta(\omega)$ denotes the Dirac delta distribution. Ideally, we would like to recover iTFR as much as possible.

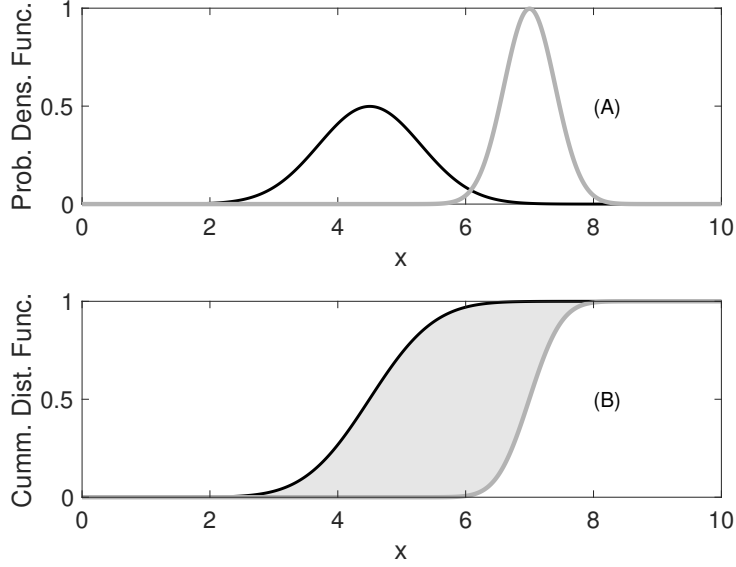


FIGURE 7. Illustration of the optimal transport distance (OTD). In (A), the black and the grey lines show two probability density functions (PDFs), respectively, and their corresponding cumulative distribution functions (CDFs) are shown in (B). The shaded area shows the OTD between these two probability measures.

To assess the performance of different algorithms in recovering the iTFR, we follow the suggestion in Daubechies *et al.* (2016) and calculate the optimal transport distance (OTD) between the iTFR and each T-F representation, respectively. The OTD is sometimes called the earth mover distance, and is associated with the Monge’s optimal transport problem Villanici (2003), which provides a way to measure similarity between probability distributions. Numerically, the OTD can be calculated in the following way Villanici (2003): for two probability measures μ and ν defined on \mathbb{R} , let $f_\mu(x) = \int_{-\infty}^x d\mu$ denote the cumulative distribution function of μ (and analogously for f_ν). Then, the OTD is defined as

$$(19) \quad d_{\text{OT}}(\mu, \nu) = \int_{\mathbb{R}} |f_\mu(x) - f_\nu(x)| dx.$$

In the plain language, the OTD is the minimal amount of “effort” (in the unit of mass times distance) that is required to transfer an amount of mass from several locations to other locations. Fig. 7 illustrates this idea, and the OTD equals to the area bounded between two cumulative distribution functions, as it is defined in Eq. (19). Note that the OTD not only captures the distance (in the x -direction) between the peaks of distributions, but is also affected by the width of the distributions.

In the context of comparing different T-F representations against the ideal one (which has an infinitely narrow width), the OTD thus allows us not only to measure the degree of concentration of each T-F representation, but also its correctness in estimating the

true IF. To evaluate the goodness of T-F representations for TE or SFOAEs, previous work has used the mean or mean-square distance between the maximum location and the ground-truth location as the performance metric Shera and Bergevin (2012); Biswal and Mishra (2017). This kind of performance metric naturally requires a pre-filtering step in the T-F plane to ensure that only the first-reflection component remains in the T-F plane. Note that OTD can be viewed as a generalization of such performance metric which uses all density information for the purpose while not requiring pre-filtering. Thus, the OTD is chosen here as a way to evaluate how accurately the concentration of the iTFR is captured by different algorithms.

Specifically, for each fixed time t , the T-F representation obtained via each algorithm is treated as a probability measure on frequency ω . Note that in general at each time t , the T-F representation does not have integral 1. Thus, the T-F representation is normalized first. Then, the OTD between the obtained T-F representation and the iTFR at time t is calculated, and its average over all time is reported as a measurement of accuracy of analysis. The results of analyzing the afore-mentioned signal by different methods, each with 30 realizations of noise, are reported in Table 2 in terms of the OTD.

4. DISCUSSION

In this section, we would like to suggest a view based on Eq. (13) and the approximation given in Eq. (16) to argue that TEOAE is intrinsically hard to analyze even when just considering the first-reflection component $r(t)$. We wish to propose that the expansion by IMT functions is thus an appropriate way to model TEOAE signals when the situation is further complicated by internal reflection components and SSOAEs. The performance of SST and ConceFT has been reported in comparison with several existing methods in the field, so limitation of the present methods can be discussed, and a few future research directions will be pointed out.

4.1. Why is TEOAE difficult to analyze? An insight from Eq. (16). The expression in Eq. (16) predicts that a tone burst centered at a particular frequency ω_b is anticipated to evoke an OAE component that returns around the time $t = E\{\tau_g(\omega_b)\} \propto \omega_b^{-1}$; further, the amplitude of that component would be scaled by a complex-valued gain $R(\omega_b)$. This result is rather simple to interpret, and since any transient and broad-band stimulus can be regarded as a superposition of narrow sub-band signals, Eq. (16) essentially predicts that the first-reflection component of TEOAE will behave like amplitude modulated *chirps*.

However, the approximation relies on one crucial assumptions — the wavenumber-domain representation $\tilde{\rho}(k)$ of the excitation pattern $\rho(x)$ must be sufficiently concentrated around its peak $k = 4\pi/\Lambda$ so that Eq. (30) can be simplified. It is rather straightforward to show that the 2nd-moment of the function $\tilde{\rho}(k)$ is equal to $1/(\Delta x)^2$. Thus, similar to how the Q-factor is defined in the frequency domain as the center frequency divided by the bandwidth, a k -domain factor can be defined for $\tilde{\rho}(k)$ and its value is $Q = 4\pi(\Delta x)/\Lambda$. A numerical investigation is given next to illustrate how the goodness of approximation in Eq. (16) depends on Q .

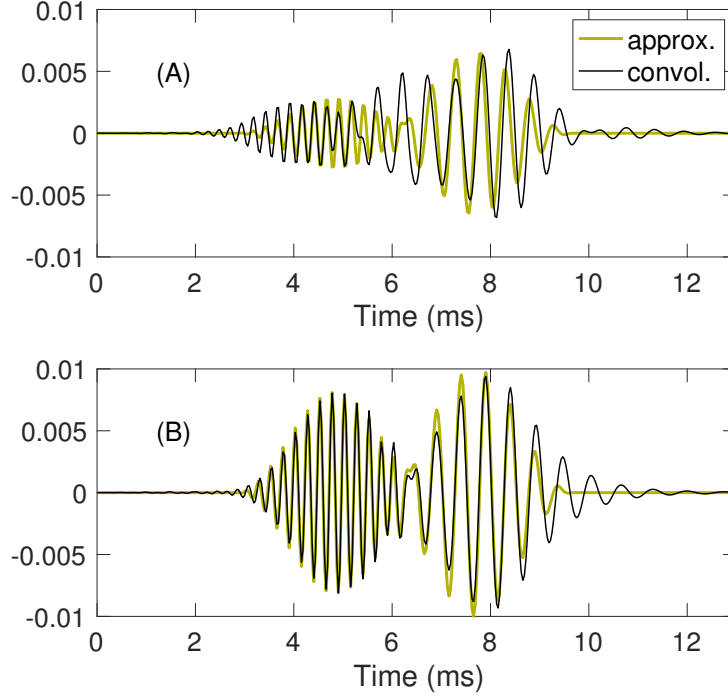


FIGURE 8. (Color online) Accuracy of approximation by Eq. (16) depends on the factor $Q = 4\pi(\Delta x/\Lambda)$. **(A)** $\Delta x/\Lambda = 0.5$, the default value in this paper. **(B)** Goodness of fitting is better when $\Delta x/\Lambda = 2.0$.

Here, a “two-tone-burst” stimulus $g(t)$ is prepared by applying a 4-ms Hann window to a mixture of two tones with $\nu_1 = 4.0$ kHz and $\nu_2 = 2.0$ kHz; that is, $g(t) = h(t)(g_1(t) + g_2(t))$ where $g_1(t) = \exp(i2\pi\nu_1 t)$, $g_2(t) = \exp(i2\pi\nu_2 t)$, and $h(t)$ denotes the Hann window with a support from $t = 0$ to 4 ms. Then, the precise first-reflection TEOAE component is calculated by $b(t) = g(t) * r(t)$, where $*$ denotes convolution in time. Additionally, an approximation $\hat{b}(t)$ based on Eq. (16) is calculated as follows,

$$(20) \quad \hat{b}(t) = C'' \sum_{j=1,2} R(2\pi\nu_j) \cdot g_j \left(t - \frac{2l}{\Lambda\nu_j} \right)$$

Figure 8 compares $\hat{b}(t)$ and $b(t)$. Panel (A) is obtained by setting $\Delta x/\Lambda$ as 0.5, a rather high value compared to 0.22 suggested in the literature (e.g., Shera and Bergevin, 2012), and panel (B) shows the result when $\Delta x/\Lambda = 2.0$, which is unreasonably high. The thin line (labeled as ‘convol.’) shows $b(t)$ and the thick, lighter line (labeled as ‘approx.’) shows $\hat{b}(t)$. In these particular examples the ratio l/Λ is set to 5.7 so we have $C'' = e^{i(0.8\pi)}$. By inspection, the approximation is better in (B) than in (A), and this agrees with the previous argument that a higher Q factor in the k -domain should result in a better approximation.

In Fig. 8(A), note that the peak of the 4-kHz packet seems to occur at an earlier time (near 4.0 ms) than predicted by Eq. (16) at 4.85 ms, or $2l/(\Lambda\nu_1) = 2.85$ ms after

the input packet peaks at $t = 2.0$ ms. This can be regarded as an example of deviation of the group delay from its expected value, even though we have introduced a lot of crude simplifications to merely consider a single and clean reflection component from a globally scaling-symmetric and linear model. With a more realistic setting of $\Delta x/\Lambda$ at a lower value, one should expect the deviation to be larger. Thus, to model the signal appropriately, the expansion by IMT functions described in Sec. 2 perhaps provides better flexibility in characterizing what frequency components, single or multiple, are present at every moment.

If we view the TEOAE signals as a sum of IMT functions, SST and ConceFT then could be adopted to estimate the AM and IF of individual components. Methods proposed in this paper might also be helpful in extracting a robust T-F representation of real TEOAE data from individual ears with normal or impaired conditions. In particular, there has been increasing evidence that TEOAEs have significant short-latency components Goodman *et al.* (2009); Jedrzejczak *et al.* (2018) coming from locations that are basal to the characteristic places Sisto *et al.* (2015). Analyzing human data by SST and ConceFT is warranted as a future research topic.

4.2. More about the present analysis method. To compare the T-F representations in terms of their capability in preserving the “ground-truth” distribution, Table 2 shows that the following results persist across different SNR levels: ConceFT is better than 1st-order SST, followed by 2nd-order SST, CWT, and then the two bilinear methods SPWV and CWD. Results for the clean signal (SNR = 100 dB) is an exception, with SST outperforming ConceFT. When the signal is clear, it is not surprising that ConceFT performs worse. This is because two windows are used, and the second Hermit window has a wider support in the T-F plane, and this slightly blurs the T-F representation of the final result. When noise is large, due to the MT effect, ConceFT performs better than SST.

In Biswal and Mishra (2017), CWT and SST were also compared among several other T-F representation methods (STFT, EMD, and S-transform). They found that the performance of CWT was better than SST at an SNR great than 15 dB in terms of group delay estimation error over a range of frequencies (0.4 to 8 kHz). The methodology of their work and the present work differ in several ways. First, the SNR range is different. Secondly, the test signal is different; they used a coherent reflection model with different realizations of the irregularity function to generate different instances of OAE signals with internal reflections, but here we choose to use signals with known ground truth directly. It turns out that their test signals had multiple-reflection components while the test signal here contains SSOAE-like components. Third, thus the performance measure is different; the group delay after Loess smoothing Shera and Bergevin (2012) was adopted as the true answer by Biswal and Mishra, and T-F analysis methods were evaluated based on how closely the smoothed group delay can be estimated despite of noise and internal reflections. Finally but not the least important, in their work, the SST was a reassignment of CWT, but in the present research the SST is based on STFT. The difference between CWT-based SST and STFT-based SST deserves a discussion. While the dilation nature of CWT renders it suitable to better visualize the chirp like frequency latency structure of the OAEs, the phase information in the high

frequency region is more mixed up compared with that of STFT when there are multiple high frequency oscillatory components. This is because to detect the high frequency component, the wavelet needs to be scaled down, and it is equivalent to broadening the frequency band. Due to the mixed up phase information in CWT, the reassignment result in the frequency axis is worse.⁸ This is why we consider the STFT-based SST, particularly the second order SST.

Here we suggest that it might be fairer to evaluate the performance by (i) comparing CWT with STFT-based SST based on OTD, and (ii) to use the Liu and Neely (2010) kind of cochlear mechanics model to generate a signal and then evaluate performance by Loess smoothed group delay estimation. Results in Table 2 indicate that ConceFT outperforms other methods, particularly when SNR is low, and this fits the theoretical development of ConceFT. Table 2 also demonstrates the potential of ConceFT as an alternative approach to handle other challenges for T-F analyses of TEOAE, including that TEOAEs are chirp-like, that there are multiple reflections within the cochlea, and that there could be SSOAEs because of multiple hot spots of generation. Nevertheless, it does not seem that any of the afore-mentioned methods (CWT vs. SST or ConceFT in particular) has absolutely better T-F analysis performance in all aspects, and ConceFT provides a solution from a different angle in some situations. The answer to “what is the best approach” might depend on the application, and whether the goal is to estimate the smoothed group delay or to follow the details of instantaneous frequency fluctuation. A systematic study to answer this question, particularly for the real data, is needed and we expect to report our findings in the future work.

5. CONCLUSION

Because of the random nature of TEOAE and existence of multiple reflections plus SSOAEs occasionally, we propose to model any given TEOAE signal as a sum of IMT functions in favor of flexibility of signal representation. Then, SST and MT can be applied to obtain the ConceFT representation. ConceFT may have several advantages compared to commonly used and well-received methods in the OAE signal analysis field, such as CWT. First, it requires minimal prior assumptions about the underlying signal, so it is less likely to lead to erroneous interpretation. Secondly, therefore, to extract underlying information about individual components such as their IF and AM, one does not need to separate the components beforehand. Via analysis of simulated OAE-like signals under noisy conditions, we demonstrate that ConceFT indeed performs better than both the 1st-order and the 2nd-order SST, the CWT with a well-chosen mother wavelet, and two bilinear transforms, in terms of its capability to preserve the ground truth. Given the established rigor that supports the SST plus the noise robustness of

⁸When there are multiple high frequency components, the broadening frequency bands due to its dilation nature will cause mixed-up of different components, and hence the mixed-up phase information. This fact leads to the common “dyadic separation” assumption when we analyze multiple oscillatory components by CWT Daubechies *et al.* (2011). Since the reassignment step in SST is based on the phase information, due to the mixed-up phase information in CWT, the reassignment result of CWT might deviate from the right location. Since there might be multiple components in the OAE signal, we consider the STFT-based SST to avoid this possible deterioration caused by the phase mixed-up.

conceFT thanks to MT, the proposed method has the potential to capture the time-varying IF function from individual TEOAEs reliably. A reasonable follow-up for this work would be to analyze real data in both normal ears and ears with cochlea-related hearing impairment.

ACKNOWLEDGMENTS

This research was supported by the Ministry of Science and Technology of Taiwan under grant No. 105-2628-E-007-005-MY2.

APPENDIX A. GROUP DELAY IN THE MEAN SENSE

In Eq. (13), the function $\epsilon(x)$ is meant to characterize the unknown perturbation of cochlear model parameters from smooth variation (Zweig and Shera, 1995). Conceptually, the high frequency components in TEOAE should appear prior to low frequency and this could possibly be shown via calculation of group delay as a function of frequency. Here, we show that the group delay decreases against frequency *in the mean sense*; that is, due to the variability among individuals, we regard the irregularity function ϵ as a random function among different ears which follows certain statistics. Under this randomness setup, the mean of the group delay across different ears decreases as ω increases (Shera and Bergevin, 2012).

A derivation is given as follows. Let $\Phi(\omega)$ denote the phase spectrum of $R(\omega)$; i.e., $R(\omega) = |R(\omega)|e^{i\Phi(\omega)}$. Since group delay involves calculating the first derivative of Φ with respect to ω , an intermediate mathematical step would be to take logarithm in the complex domain as to “unraise” $\Phi(\omega)$ from the exponent; that is, $\log(R(\omega)) = \log|R(\omega)| + i\Phi(\omega)$. Then, taking the first derivative with respect to ω , we have

$$(21a) \quad \frac{1}{|R(\omega)|} \frac{\partial |R|}{\partial \omega} + i \frac{\partial \Phi(\omega)}{\partial \omega} = \frac{\partial \log R(\omega)}{\partial \omega}$$

$$(21b) \quad = \frac{1}{R(\omega)} \frac{\partial}{\partial \omega} \int \epsilon(x') e^{\frac{-(x'-x_p)^2}{2(\Delta x)^2}} e^{-i4\pi\left(\frac{x'-x_p}{\Lambda}\right)} dx'$$

$$(21c) \quad = \frac{1}{R(\omega)} \int \epsilon(x') \left[-\frac{(x'-x_p)}{(\Delta x)^2} + i\frac{4\pi}{\Lambda} \right] \frac{\partial x_p}{\partial \omega} \cdot e^{\frac{-(x'-x_p)^2}{2(\Delta x)^2}} e^{-i4\pi\left(\frac{x'-x_p}{\Lambda}\right)} dx'.$$

Note that Eq. (21b) is a simple application of the chain rule. Based on the log-linear relation in Eq. (14), we have

$$\partial x_p / \partial \omega = -l / \omega.$$

Substituting this into Eq. (21c), the following expression is obtained,

$$(22a) \quad \frac{\partial \log R(\omega)}{\partial \omega} = \frac{1}{R(\omega)} \frac{l}{\omega} \left[-i\frac{4\pi}{\Lambda} R(\omega) + \int \epsilon(x') H(x' - x_p, \omega) dx' \right]$$

$$(22b) \quad = -i\frac{4\pi}{\Lambda} \frac{l}{\omega} + \frac{1}{R(\omega)} \frac{l}{\omega} \int \epsilon(x') H(x' - x_p, \omega) dx',$$

where $H(x, \omega)$ is defined as follows for the convenience of notations:

$$H(y, \omega) = \frac{y}{(\Delta x)^2} e^{\frac{-y^2}{2(\Delta x)^2}} e^{-i4\pi y/\Lambda}.$$

Note that, in Eq. (22b), the integral depends on $\epsilon(x')$ and generally does not vanish. Nevertheless, if we treat ϵ as a random function and assume that $E\{\epsilon(x)\} = 0$ for all x , where $E(\cdot)$ means to take the expected value across an ensemble of ears of similar conditions, then by comparing the imaginary and real parts of Eq. (22b) and (21a), we can conclude that the following relation holds for the group delay τ_g in the mean sense,

$$(23) \quad E\{\tau_g(\omega)\} = E\left\{-\frac{\partial \Phi}{\partial \omega}\right\} = \frac{4\pi}{\Lambda} \frac{l}{\omega} = \frac{4\pi}{\Lambda} \left(-\frac{\partial x_p}{\partial \omega}\right).$$

Note that $E\{\tau_g(\omega)\}$ monotonically decreases against ω in Eq. (23). For $\tau_g(\omega)$ in an individual ear, the relation should deviate from mean due to the presence of the integral term in Eq. (22b).

When only the data from one single ear is available, the alternative way to estimate the mean group delay is by smoothing over frequency. Interested readers can refer to Keefe (2012) and Shera and Bergevin (2012) for a thorough evaluation of various smoothing methods.

APPENDIX B. FORMULATION IN THE WAVENUMBER DOMAIN

In this subsection an interpretation of coherent reflection from the spatial frequency domain Zweig and Shera (1995) is studied. By transforming to the wavenumber domain and interchanging the order of integration, it turns out that approximation can be made for the purpose of discussing time-domain properties of TEOAEs (to be revealed in Sec. C and D).

First, by defining $\rho(u) = e^{\frac{-u^2}{2(\Delta x)^2}} e^{-i4\pi \frac{u}{\Lambda}}$ and applying a change-of-variable $y = x - x'$, Eq. (13) can be re-written as,

$$(24) \quad R(\omega) = \int \epsilon(y + x_p) \rho(y) dy.$$

Now, let us assume that $\tilde{\epsilon}(k)$ is the spatial Fourier transform of $\epsilon(x)$ so we have

$$(25) \quad \epsilon(y) = \frac{1}{2\pi} \int \tilde{\epsilon}(k) e^{iky} dk,$$

where the variable k is referred to as the wavenumber, or the spatial frequency. Combining the previous two equations, we have the following expression for $R(\omega)$,

$$(26a) \quad R(\omega) = \frac{1}{2\pi} \int \left(\int \tilde{\epsilon}(k) e^{ik(y+x_p)} dk \right) \rho(y) dy$$

$$(26b) \quad = \frac{1}{2\pi} \int \left(\int \rho(y) e^{iky} dy \right) e^{ikx_p} \tilde{\epsilon}(k) dk$$

$$(26c) \quad = \frac{1}{2\pi} \int \tilde{\rho}^*(k) \tilde{\epsilon}(k) e^{ikx_p(\omega)} dk,$$

where $\tilde{\rho}(k) = \int \rho(y)e^{-iky}dy$ denotes the spatial Fourier transform of ρ , and $\tilde{\rho}^*(k) = \tilde{\rho}(-k)$.

Equation (26c) has a *spatial filtering* interpretation — $\tilde{\epsilon}(k)$ is spatially filtered by $\tilde{\rho}^*(k)$, which has a peak magnitude at $k = 4\pi/\Lambda$ and a spatial bandwidth of $1/\Delta x$ (Zweig and Shera, 1995). In this sense, we can say that as much as reflection is concerned, the most significant contribution stems from $\tilde{\rho}^*(k)\tilde{\epsilon}(k)$ at spatial frequency $k = 4\pi/\Lambda$.

APPENDIX C. OAE EVOKED BY A NARROWBAND STIMULUS

Now let us start from Eq. (26c) and discuss the special case of OAE evoked by a *tone burst* (TB). Here, a tone burst $g(t)$ refers to a pure tone shaped in time by a window function so its spectrum is narrow-band around its center frequency ω_b . TBs have long been used in human and animal experiments (Neely *et al.*, 1988; Konrad-Martin and Keefe, 2003; Siegel *et al.*, 2011) to study the properties of the cochlea. Denoting the Fourier transform of $g(t)$ as $G(\omega)$, the first-reflection part of tone burst-evoked OAE (TBOAE) spectrum can be written as follows,

$$(27) \quad B(\omega) = R(\omega)G(\omega),$$

and thus its inverse Fourier transform $b(t)$ is

$$(28) \quad b(t) = \frac{1}{4\pi^2} \int \tilde{\rho}^*(k)\tilde{\epsilon}(k) \left(\int e^{ikx_p} G(\omega) e^{i\omega t} d\omega \right) dk.$$

Note that x_p is a logarithmic function of ω so it seems that a close-form expression does not exist for the integral $\int e^{ikx_p(\omega)} G(\omega) e^{i\omega t} d\omega$. To continue, we utilize the assumption that $G(\omega)$ is narrow-banded. More precisely, we are going to assume that $\int e^{ikx_p(\omega)} G(\omega) e^{i\omega t} d\omega$ can be approximated by calculating within a narrowband $\omega \in [\omega_b - \delta, \omega_b + \delta]$.

Then, by $x_p(\omega) = \log \frac{\omega_0}{\omega_b} - \log \frac{\omega}{\omega_b}$, the following derivation can be made,

$$(29a) \quad \begin{aligned} & \int e^{ikx_p} G(\omega) e^{i\omega t} d\omega \\ & \approx \int_{\omega_b - \delta}^{\omega_b + \delta} e^{ikl \left(\log \frac{\omega_0}{\omega_b} - \log \frac{\omega}{\omega_b} \right)} G(\omega) e^{i\omega t} d\omega \end{aligned}$$

$$(29b) \quad = C(k) \int_{\omega_b - \delta}^{\omega_b + \delta} e^{-ikl \log(1+u)} G(\omega) e^{i\omega t} d\omega \quad \left(\text{Here let } u = \frac{\omega}{\omega_b} - 1 \right)$$

$$(29c) \quad \approx C'(k) \int_{\omega_b - \delta}^{\omega_b + \delta} e^{-ikl \frac{\omega}{\omega_b}} e^{i\omega t} G(\omega) d\omega$$

$$(29d) \quad \approx 2\pi C'(k) g \left(t - \frac{kl}{\omega_b} \right),$$

where $C'(k) = e^{ikl[1+\log(\omega_0/\omega_b)]}$ does not depend on ω and (29c) comes from Taylor's expansion around ω_b , for $G(\omega)$ is assumed to be narrow-banded.

Substituting (29d) into Eq. (28), we have the following approximation for $b(t)$, the first-reflection component of the TBOAE signal,

$$(30) \quad b(t) \approx \frac{1}{2\pi} \int C'(k) \tilde{\rho}^*(k) \tilde{\epsilon}(k) g\left(t - \frac{kl}{\omega_b}\right) dk.$$

Note that, if $\Delta x/\Lambda$ is sufficiently large, we can assume that $\tilde{\rho}^*(k)$ is concentrated around $k = 4\pi/\Lambda$ so the integral in Eq. (30) can be regarded as mostly contributed by a short interval $\theta = [4\pi/\Lambda - \delta_k, 4\pi/\Lambda + \delta_k]$, where $g(t - kl/\omega_b) \approx g(t - kl/\omega_b)|_{k=4\pi/\Lambda}$. Therefore, the following approximation for Eq. (30) is obtained,

$$(31) \quad b(t) \approx \left(\int e^{ikl} e^{ikx_p(\omega_b)} \tilde{\rho}^*(k) \tilde{\epsilon}(k) dk \right) \cdot g\left(t - \frac{4\pi l}{\Lambda \omega_b}\right).$$

This expression shows some insights. First, the stimulus $g(t)$, which has a center frequency of ω_b , is approximately delayed by $4\pi l/(\omega_b \Lambda)$ when emitting out of the cochlea. This delay term agrees with our previous derivation in Eq. (23) that was obtained from a rather different angle. Secondly, assuming that the integral in Eq. (31) is again dominated by a short interval $\theta = [4\pi/\Lambda - \delta_k, 4\pi/\Lambda + \delta_k]$, then $b(t)$ can be re-arranged as Eq. (16).

APPENDIX D. BREAKING TEOAE INTO SUB-BAND TBOAE

The previous derivation assumes that the stimulus is narrow-band and the crude approximation in Eq. (29c) assumes that higher order terms in the Taylor series expansion of $\log(1 + u)$ can be omitted. In this section, we attempt to loosen the narrow-band requirement on the stimulus.

The following Paley-Littlewood type decomposition is considered Stein (1993). Consider η to be a smooth function that is compactly supported on $[-2, 2]$ (Hz)⁹ so that $\eta(x) = 1$ when $x \in [-1, 1]$ (Hz). Denote $\psi_j(x) = \eta(2^{-j}x) - \eta(2^{-j+1}x)$ for $j \in \mathbb{Z}$. ψ_j could be viewed as a band-pass filter, which has the support over $[2^{j-1}, 2^{j+1}]$ (Hz). By a direct calculation, we see that $\eta(2^{-L_0+1}x) + \sum_{j=L_0}^{\infty} \psi_j(x) = 1$ for all x , where $L_0 \in \mathbb{Z}$. By the Paley-Littlewood type decomposition, the R function in the Fourier domain can be rewritten as

$$(32) \quad R(\omega) = R(\omega) \left[\eta(2^{-L_0+1}\omega) + \sum_{j=L_0}^{\infty} \psi_j(\omega) \right] = R(\omega) \eta(2^{-L_0+1}\omega) + \sum_{j=L_0}^{\infty} R(\omega) \psi_j(\omega),$$

where L_0 is chosen to be a sufficiently low integer such that the support for $R(\omega) \eta(2^{-L_0+1}\omega)$ falls below the human hearing range and the term can thus be ignored. On the other hand, we model the incident wave to have a wide but compact support in the Fourier domain so that its Fourier transform is $\sum_{j \leq L_1} \psi_j$, where $L_1 \geq 1$. By these assumptions, the TEOAE signal have the following expansion:

$$(33) \quad P(t) = \int R(\omega) \sum_{j=L_0}^{L_1} \psi_j(\omega) e^{i\omega t} d\omega = \sum_{j=L_0}^{L_1} s_j.$$

⁹The exact unit here is not important for mathematical formulation, but to be consistent with notations, here we arbitrarily assign the unit Hz.

where in the time domain we have

$$(34) \quad s_j(t) := \mathcal{F}^{-1}[R(\omega)\psi_j(\omega)](t),$$

which can be regarded as the j -th TBOAE with the dominant frequency around 2^j Hz.

Due to the log term appearing in the exponential, to better understand the TEOAE signal, we follow the approximation idea in Section C. Rewrite the j -th TBOAE as

$$(35) \quad s_j(t) = \frac{1}{2\pi} \int \tilde{\rho}^*(k) \tilde{\epsilon}(k) \left[\int e^{ix_p(\omega)k} \psi_j(\omega) e^{i\omega t} d\omega \right] dk,$$

where the integration inside the bracket could be rewritten as

$$(36) \quad \int e^{ix_p(\omega)k} \psi_j(\omega) e^{i\omega t} d\omega = \int e^{-i(kl \log \frac{\omega}{\omega_0} - t\omega)} \psi_j(\omega) d\omega.$$

Recall that ψ_j is supported on $[2^{j-1}, 2^{j+1}]$ Hz. By denoting $\Omega_j := 2^j$ and applying Taylor's expansion, we could approximate $kl \log \frac{\omega}{\omega_0}$ by $kl[\log \frac{\Omega_j}{\omega_0} - \frac{1}{\Omega_j}(\Omega_j - \omega) - \frac{1}{2\tilde{\omega}^2}(\Omega_j - \omega)^2]$, where $\tilde{\omega}$ is between Ω_j and ω . As a result, by ignoring the second order term, we have the following approximation

$$(37) \quad \begin{aligned} \int e^{-i(kl \log \frac{\omega}{\omega_0} - t\omega)} \psi_j(\omega) d\omega &\approx \int e^{i(kl[\log \frac{\Omega_j}{\omega_0} + \frac{1}{\Omega_j}(\Omega_j - \omega)] + t\omega)} \psi_j(\omega) d\omega \\ &= g_j \left(t - \frac{kl}{\Omega_j} \right) e^{ikl[\log \frac{\Omega_j}{\omega_0} + 1]}, \end{aligned}$$

where $g_j(t) := \mathcal{F}^{-1}(\psi_j)(t)$, and hence approximate s_j by

$$(38) \quad s_j^{(L)}(t) := \frac{1}{2\pi} \int \tilde{\rho}^*(k) \tilde{\epsilon}(k) g_j \left(t - \frac{kl}{\Omega_j} \right) e^{ikl[\log \frac{\Omega_j}{\omega_0} + 1]} dk.$$

By assumption, $\tilde{\rho}^*(k)$ decays exponentially fast and is concentrated on $\frac{4\pi}{\Lambda}$ and $\tilde{\epsilon}(k)e^{ikl[\log \frac{\Omega_j}{\omega_0} + 1]}$ is bounded. Therefore, by a direct approximation, $s_j^{(L)}(t)$ becomes

$$(39) \quad \begin{aligned} s_j^{(L)}(t) &\approx \frac{1}{2\pi} \left[\int \tilde{\rho}^*(k) \tilde{\epsilon}(k) e^{ikl \log \frac{\Omega_j}{\omega_0}} dk \right] g_j \left(t - \frac{4\pi l}{\Lambda \Omega_j} \right) e^{i\frac{4\pi}{\Lambda} l} \\ &= \frac{1}{2\pi} R(\Omega_j) 2^j g_1 \left(2^j t - \frac{4\pi l}{\Lambda} \right) e^{i\frac{4\pi}{\Lambda} l} \end{aligned}$$

where we use the fact that

$$(40) \quad g_j(t) = \frac{1}{2\pi} \int_{2^{j-1}}^{2^{j+1}} [\eta(2^{-j}\omega) - \eta(2^{-j+1}\omega)] e^{i\omega t} d\omega = \frac{2^j}{2\pi} \int_{1/2}^2 \psi_1(\omega) e^{-i2^j \omega t} d\omega = 2^j g_1(2^j t),$$

which is an oscillatory signal (or could be understood as a dilated wavelet). This approximation suggests that we could well approximate a TBOAE as a “time lagged” reflected signal, where the reflected signal comes from an inner ear that has a locally

linearized tonotopic mapping relation. As a result, we have the following approximation

$$(41) \quad P(t) \approx \frac{1}{2\pi} e^{i\frac{4\pi}{\Lambda}l} \sum_{j=L_0}^{L_1} R(\Omega_j) 2^j g_1 \left(2^j t - \frac{4\pi l}{\Lambda} \right),$$

where we view the TEOAE as a summation of a sequence of latent TBOAE of different frequencies, and the latency depends on the frequency of the TBOAE. Note that the TEOAE has a higher frequency oscillation in the beginning with a stronger power and a short period, and has a lower frequency oscillation later with a weaker power and a longer period. The relationship between the frequency and latency is inverse to each other, and the decay of the amplitude depends on the decay of R . To sum up, this model depicts the fundamental feature of first-reflection component of TEOAE — as an oscillatory signal, and both the amplitude and the frequency decrease as time goes.

REFERENCES

- Auger, F., and Flandrin, P. (1995). “Improving the readability of time-frequency and time-scale representations by the reassignment method,” *IEEE Trans. Signal Process.* **43**(5), 1068–1089.
- Biswal, M., and Mishra, S. (2017). “On reliable time-frequency characterization and delay estimation of stimulus frequency otoacoustic emissions,” in *Proc. Mechanics of Hearing Workshop*, Ontario, Canada, pp. 526–531.
- Chen, Y.-C., Cheng, M.-Y., and Wu, H.-T. (2014). “Nonparametric and adaptive modeling of dynamic seasonality and trend with heteroscedastic and dependent errors,” *J. Roy. Stat. Soc. B* **76**, 651–682.
- Choi, Y.-S., Lee, S.-Y., Parham, K., Neely, S. T., and Kim, D. O. (2008). “Stimulus-frequency otoacoustic emission: measurements in humans and simulations with an active cochlear model,” *J. Acoust. Soc. Amer.* **123**(5), 2651–2669.
- Daubechies, I. (1988). “Time-frequency localization operators: A geometric phase space approach,” *IEEE Trans. Inform. Theory* **34**, 605–612.
- Daubechies, I., Lu, J., and Wu, H.-T. (2011). “Synchrosqueezed wavelet transforms: An empirical mode decomposition-like tool,” *Appl. Comput. Harmon. Anal.* **30**, 243–261.
- Daubechies, I., Wang, Y., and Wu, H.-T. (2016). “Conceft: Concentration of frequency and time via a multitapered synchrosqueezed transform,” *The Royal Soc. Publishing: Phil. Trans. A* **374**, 20150193.
- Flandrin, P. (1999). *Time-frequency/time-scale analysis*, **10** of *Wavelet Analysis and its Applications* (Academic Press Inc., San Diego), pp. xii+386.
- Goodman, S. S., Fitzpatrick, D. F., Ellison, J. C., Jesteadt, W., and Keefe, D. H. (2009). “High-frequency click-evoked otoacoustic emissions and behavioral thresholds in humans,” *J. Acoust. Soc. Amer.* **125**, 1014–1032.
- Greenwood, D. D. (1990). “A cochlear frequency-position function for several species – 29 years later,” *J. Acoust. Soc. Amer.* **87**, 2592–2605.
- Huang, N. E., Shen, Z., Long, S. R., Wu, M., Shih, H., Zheng, Q., Yen, N.-C., Tung, C. C., and Liu, H. H. (1998). “The empirical mode decomposition and the Hilbert

- spectrum for nonlinear and non-stationary time series analysis,” *Proc. R. Soc. Lond. A* **454**(1971), 903–995.
- Huang, Z., Zhang, J., Zhao, T., and Sun, Y. (2016). “Synchrosqueezing s-transform and its application in seismic spectral decomposition,” *IEEE Transactions on Geoscience and Remote Sensing* **54**(2), 817–825.
- Janusauskas, A., Marozas, V., Engdahl, B., Hoffman, H. J., Svensson, O., and Sörnmo, L. (2001). “Otoacoustic emissions and improved pass/fail separation using wavelet analysis and time windowing,” *Medical & biological engineering & computing* **39**(1), 134–9.
- Jedrzejczak, W., Kochanek, K., and Skarzynski, H. (2018). “Otoacoustic emissions from ears with spontaneous activity behave differently to those without: Stronger responses to tone bursts as well as to clicks,” *PLoS One* **13**, e0192930, 18 pages.
- Jedrzejczak, W., Kwaskiewicz, K., Blinowska, K., Kochanek, K., and Skarzynski, H. (2009). “Use of the matching pursuit algorithm with a dictionary of asymmetric waveforms in the analysis of transient evoked otoacoustic emissions,” *J. Acoust. Soc. Amer.* **126**, 3137–3146.
- Keefe, D. H. (2012). “Moments of click-evoked otoacoustic emissions in human ears: Group delay and spread, instantaneous frequency and bandwidth,” *J. Acoust. Soc. Amer.* **132**, 3319–3350.
- Kemp, D. T. (1978). “Stimulated acoustic emissions from within the human auditory system,” *J. Acoust. Soc. Amer.* **64**, 1386–1391.
- Kodera, K., Gendrin, R., and Villedary, C. (1978). “Analysis of time-varying signals with small bt values,” *IEEE Trans. Acoust., Speech, Signal Processing* **26**(1), 64 – 76.
- Konrad-Martin, D., and Keefe, D. H. (2003). “Time-frequency analyses of transient-evoked stimulus-frequency and distortion-product otoacoustic emissions: Testing cochlear model predictions,” *J. Acoust. Soc. Amer.* **114**, 2021–2043.
- Kopsinis, Y., and McLaughlin, S. (2009). “Development of EMD-based denoising methods inspired by wavelet thresholding,” *IEEE Trans. Signal Process.* **57**, 1351–1362.
- Kowalski, M., Meynard, A., and Wu, H.-T. (2018). “Convex optimization approach to signals with fast varying instantaneous frequency,” *Applied and Computational Harmonic Analysis* **44**(1), 89 – 122.
- Lin, Y.-T., Wu, H.-T., Tsao, J., Yien, H.-W., and Hseu, S.-S. (2014). “Time-varying spectral analysis revealing differential effects of sevoflurane anaesthesia: non-rhythmic-to-rhythmic ratio,” *Acta Anaesthesiol Scand* **58**, 157–167.
- Liu, Y.-W., and Liu, T.-C. (2016). “Quasilinear reflection as a possible mechanism for suppressor-induced otoacoustic emission,” *J. Acoust. Soc. Amer.* **140**, 4193–4203.
- Liu, Y.-W., and Neely, S. T. (2009). “Outer hair cell electromechanical properties in a nonlinear piezoelectric model,” *J. Acoust. Soc. Amer.* **126**, 751–761.
- Liu, Y.-W., and Neely, S. T. (2010). “Distortion-product emissions from a cochlear model with nonlinear mechano-electrical transduction in outer hair cells,” *J. Acoust. Soc. Amer.* **127**, 2420–2432.
- Mishra, S. K., and Biswal, M. (2016). “Time-frequency decomposition of click evoked otoacoustic emissions in children,” *Hearing Research* **335**, 161 – 178.

- Moleti, A., Longo, F., and Sisto, R. (2012). “Time-frequency domain filtering of evoked otoacoustic emissions,” *J. Acoust. Soc. Amer.* **132**(4), 2455–2467.
- Moleti, A., Sisto, R., Tognola, G., Parazzini, M., Ravazzani, P., and Grandori, F. (2005). “Otoacoustic emission latency, cochlear tuning, and hearing functionality in neonates,” *J. Acoust. Soc. Amer.* **118**, 1576–1584.
- Mountain, D. C., and Hubbard, A. E. (1994). “A piezoelectric model of outer hair cell function,” *J. Acoust. Soc. Amer.* **95**, 350–354.
- Neely, S. T. (1985). “Mathematical modeling of cochlear mechanics,” *J. Acoust. Soc. Amer.* **78**, 345–352.
- Neely, S. T. (1993). “A model of cochlear mechanics with outer hair cell motility,” *J. Acoust. Soc. Amer.* **94**, 137–146.
- Neely, S. T., Norton, S. J., Gorga, M. P., and Jesteadt, W. (1988). “Latency of auditory brain-stem responses and otoacoustic emissions using tone-burst stimuli,” *J. Acoust. Soc. Amer.* **83**, 652–656.
- Notaro, G., Al-Maamury, A. M., Moleti, A., and Sisto, R. (2007). “Wavelet and matching pursuit estimates of the transient-evoked otoacoustic emission latency,” *J. Acoust. Soc. Amer.* **122**(6), 3576–85.
- Oberlin, T., Meignen, S., and Perrier, V. (2015). “Second-Order Synchrosqueezing Transform or Invertible Reassignment ? Towards Ideal Time-frequency Representations,” *IEEE Transactions on Signal Processing* **63**(5), 1335–1344.
- Percival, D. B., and Walden, A. T. (1993). *Spectral Analysis for Physical Applications: Multitaper and Conventional Univariate Techniques* (Cambridge University Press).
- Rhode, W. S. (1978). “Some observations on cochlear mechanics,” *J. Acoust. Soc. Amer.* **64**, 158–176.
- Ricaud, B., and Torresani, B. (2014). “A survey of uncertainty principles and some signal processing applications,” *Advances in Computational Mathematics* **40**(3), 629–650.
- Schroeder, M. R. (1973). “An integrable model of the basilar membrane,” *J. Acoust. Soc. Amer.* **53**, 429–434.
- Shera, C., and Bergevin, C. (2012). “Obtaining reliable phase-gradient delays from otoacoustic emission data,” *J. Acoust. Soc. Amer.* **132**, 927–943.
- Shera, C. A., Guinan, J. J., and Oxenham, A. J. (2010). “Otoacoustic estimation of cochlear tuning: Validation in the chinchilla,” *J. Assoc. Res. Otolaryngol.* **11**, 343–365.
- Shera, C. A., Guinan, Jr, J. J., and Oxenham, A. J. (2002). “Revised estimates of human cochlear tuning from otoacoustic and behavioral measurements,” *Proc. Natl. Acad. Sci.* **99**, 3318–3323.
- Siegel, J. H., Charaziak, K., and Cheatham, M. A. (2011). “Transient- and tone-evoked otoacoustic emissions in three species,” *AIP Conf. Proc.* **1403**, 307–314.
- Sisto, R., and Moleti, A. (2007). “Transient evoked otoacoustic emission latency and cochlear tuning at different stimulus levels,” *J. Acoust. Soc. Amer.* **122**, 2183–2190.
- Sisto, R., Moleti, A., and Shera, C. A. (2015). “On the spatial distribution of the reflection sources of different latency components of otoacoustic emissions,” *J. Acoust. Soc. Amer.* **137**(2), 768–776.

- Stein, E. M. (1993). *Harmonic Analysis, Volume 43: Real-variable Methods, Orthogonality, and Oscillatory Integrals* (Princeton University Press).
- Talmadge, C. L., Tubis, A., Long, G. R., and Piskorski, P. (1998). “Modeling otoacoustic emission and hearing threshold fine structures,” *J. Acoust. Soc. Amer.* **104**, 1517–1543.
- Talmadge, C. L., Tubis, A., Long, G. R., and Tong, C. (2000). “Modeling the combined effects of basilar membrane nonlinearity and roughness on stimulus frequency otoacoustic emission fine structure,” *J. Acoust. Soc. Amer.* **108**, 2911–2932.
- Thakur, G., Brevdo, E., Fuckar, N. S., and Wu, H.-T. (2013). “The synchrosqueezing algorithm for time-varying spectral analysis: robustness properties and new paleoclimatic applications,” *Signal Processing* **93**(5), 1079–1094.
- Tognola, G., Grandori, F., and Ravazzani, P. (1997). “Time-frequency distributions of click- evoked otoacoustic emissions,” *Hearing Research* **106**, 112–122.
- Tognola, G., Parazzini, M., De Jager, P., Brienesse, P., Ravazzani, P., and Grandori, F. (2001). “Cochlear maturation and otoacoustic emissions in preterm infants: a time – frequency approach,” in *2001 Proceedings of the 23rd Annual EMBS International Conference, October 25-28, Istanbul, Turkey*, Vol. 199, pp. 71–80.
- Verhulst, S., Dau, T., and Shera, C. A. (2012). “Nonlinear time-domain cochlear model for transient stimulation and human otoacoustic emission,” *J. Acoust. Soc. Amer.* **132**(6), 3842–3848.
- Villanici, C. (2003). *Topics in Optimal Transportation* (Graduate Studies in Mathematics, American Mathematical Society).
- Wu, H.-T. (2011). “Adaptive Analysis of Complex Data Sets,” Ph.D. thesis, Princeton University.
- Xiao, J., and Flandrin, P. (2007). “Multitaper Time-Frequency Reassignment for Nonstationary Spectrum Estimation and Chirp Enhancement,” *IEEE Trans. Signal Process.* **55**, 2851–2860.
- Yakov, S. G. (1992). *Probability Theory: an introductory course* (Springer).
- Zweig, G., and Shera, C. A. (1995). “The origin of periodicity in the spectrum of evoked otoacoustic emissions,” *J. Acoust. Soc. Amer.* **98**, 2018–2047.

HAU-TIENG WU, DEPARTMENT OF MATHEMATICS AND DEPARTMENT OF STATISTICAL SCIENCE,
DUKE UNIVERSITY, NC, 27705, USA

YI-WEN LIU, DEPARTMENT OF ELECTRICAL ENGINEERING, NATIONAL TSING HUA UNIVERSITY,
HSINCHU 30013, TAIWAN

E-mail address: ywliu@ee.nthu.edu.tw